Journal of Medicinal Chemistry

Article

Cite This: J. Med. Chem. 2018, 61, 4348−4369

pubs.acs.org/jmc

# Optimization of Selective Mitogen-Activated Protein Kinase Interacting Kinases 1 and 2 Inhibitors for the Treatment of Blast Crisis Leukemia

Haiyan Yang,[†] Lohitha Rao Chennamaneni,[‡] Melvyn Wai Tuck Ho,[†] Shi Hua Ang,[†] Eldwin Sum Wai Tan,[†] Duraiswamy Athisayamani Jeyaraj,[†] Yoon Sheng Yeap,[†] Boping Liu,[†] Esther Hq Ong,[†] Joma Kanikadu Joy,[†] John Liang Kuan Wee,[†] Perlyn Kwek,[†] Priya Retna,[†] Nurul Dinie,[†] Thuy Thi Hanh Nguyen,[†] Shi Jing Tai,[†] Vithya Manoharan,[†] Vishal Pendharkar,[†] Choon Bing Low,[†] Yun Shan Chew,[†] Susmitha Vuddagiri,[†] Kanda Sangthongpitag,[†] Meng Ling Choong,[†] May Ann Lee,[†] Srinivasaraghavan Kannan,[§] Chandra S. Verma,[§,∥,⊥] Anders Poulsen,[†] Sharon Lim,[#] Charles Chuah,[#] Tiong Sin Ong,[#,⊗] Jeffrey Hill,[†] Alex Matter,[†] and Kassoum Nacro*[,†]

[†]Experimental Therapeutics Centre (ETC), A*STAR, 31 Biopolis Way, Nanos #03-01, 138669 Singapore

[‡]Organic Chemistry, Institute of Chemical and Engineering Sciences (ICES), A*STAR, 8 Biomedical Grove, Neuros, #07-01, 138665 Singapore

[§]Bioinformatics Institute (BII), A*STAR, 30 Biopolis Street, #07-01 Matrix, 138671 Singapore

[∥]School of Biological Sciences, Nanyang Technological University, 60 Nanyang Drive, 637551 Singapore

[⊥]Department of Biological Sciences, National University of Singapore, 14 Science Drive 4, 117543 Singapore

[#]Duke-NUS Medical School, 8 College Road, 169857 Singapore

[⊗]Department of Medicine, Duke University Medical Center, Durham, North Carolina 27710, United States

Supporting Information

**ABSTRACT:** Chronic myeloid leukemia (CML) is a myeloproliferative disease caused by *bcr-abl1*, a constitutively active tyrosine kinase fusion gene responsible for an abnormal proliferation of leukemic stem cells (LSCs). Inhibition of BCR-ABL1 kinase activity offers long-term relief to CML patients. However, for a proportion of them, BCR-ABL1 inhibition will become ineffective at treating the disease, and CML will progress to blast crisis (BC) CML with poor prognosis. BC-CML is often associated with excessive phosphorylated eukaryotic translation initiation factor 4E (eIF4E), which renders LSCs capable of proliferating via self-renewal, oblivious to BCR-ABL1 inhibition. *In vivo*, eIF4E is exclusively phosphorylated on Ser209 by MNK1/2. Consequently, a selective inhibitor of MNK1/2 should reduce the level of phosphorylated eIF4E and re-sensitize LSCs to BCR-ABL1 inhibition, thus hindering the proliferation of BC LSCs. We report herein the structure−activity relationships and pharmacokinetic properties of a selective MNK1/2 inhibitor clinical candidate, ETC-206, which in combination with dasatinib prevents BC-CML LSC self-renewal *in vitro* and enhances dasatinib antitumor activity *in vivo*.

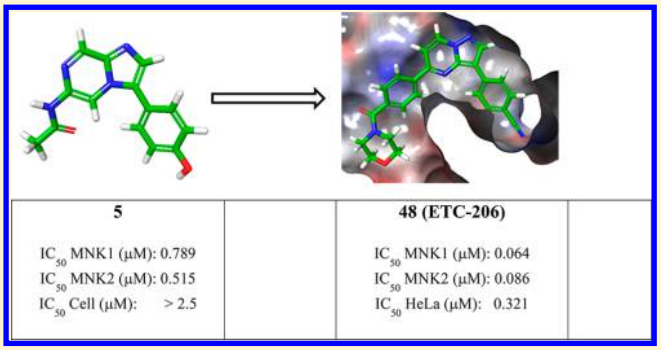


## INTRODUCTION

Messenger RNA (mRNA) translation is a highly regulated process pervasive to many biological processes, in which eukaryotic translation initiation factor 4E (eIF4E), a cap-dependent translation factor, plays a crucial role. eIF4E, one of the five MAP kinase interacting serine/threonine kinases 1 and 2 (MNK1/2) substrates,[1] is phosphorylated *in vivo* only by MNK1/2 on Ser209, and accordingly, phospho-eIF4E is not detected in Mnk1/2 knock-out mice.[2] Overexpression of phosphorylated eIF4E has been linked to inflammation,[3−5] central nervous system disorders,[6] and malignancies such as glioblastoma,[7−9] breast cancer,[10−12] pancreatic ductal adenocarcinoma,[13,14] and leukemias.[15,16] Abnormally high mRNA translation of oncogenic transcripts is thought to fuel the growth of cancers, including chronic myeloid leukemia (CML), where tumorigenic pathways are activated through eIF4E overexpression and/or phosphorylation.[17−22] Specifically, blast

Received: November 22, 2017
Published: April 23, 2018





DOI: 10.1021/acs.jmedchem.7b01714
J. Med. Chem. 2018, 61, 4348−4369

**Scheme 1. Synthesis of *N*-(3-(4-Hydroxyphenyl)imidazo[1,2-*a*]pyrazinyl)-6 Amides 4 and 5, and 6-Phenyl 8**[a]

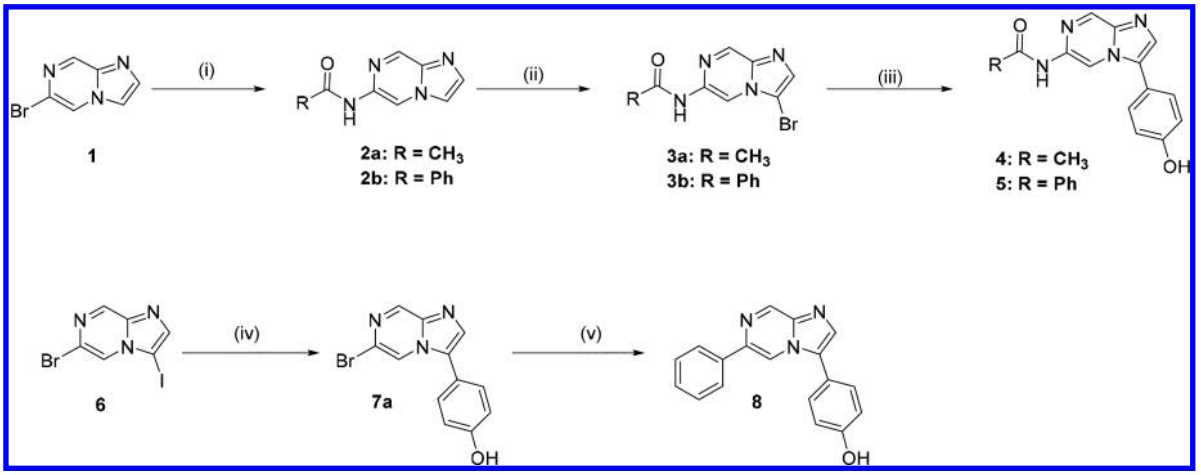


[a]Reagents and conditions: (i) acetamide or benzamide, *N*,*N*-dimethylethylenediamine, $K_2CO_3$, CuI, Toluene, 90 °C, 12 h; (ii) NBS, $CH_2Cl_2$, 1 h; (iii) (4-hydroxyphenyl)boronic acid, $Na_2CO_3$, $Pd(OAc)_2$, $P(PPh_3)_4$, 1,4-dioxane, 90 °C, 12 h; (iv) (4-hydroxyphenyl)boronic acid, $Na_2CO_3$, $Pd(PPh_3)_4$, 1,4-dioxane, 90 °C, 12 h; (v) phenylboronic acid, $Pd(dppf)_2Cl_2$, $Cs_2CO_3$, DMF, $H_2O$, 140 °C, 30 min.

**Scheme 2. Synthesis of Imidazopyrazine Analogues 19−33**[a]

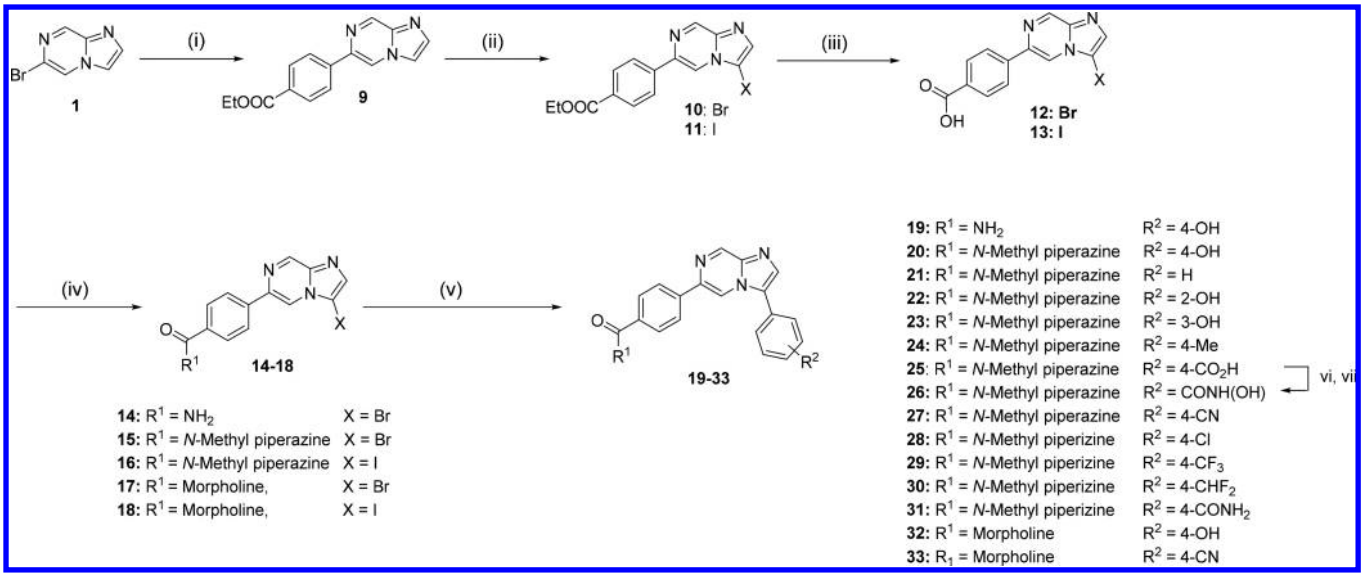


[a]Reagents and conditions: (i) (4-(ethoxycarbonyl)phenyl)boronic acid, $Pd(dppf)_2Cl_2$, $Cs_2CO_3$, toluene, 90 °C, 12 h; (ii) NBS, MeOH, $CCl_4$ or NIS, DMF; (iii) LiOH, $H_2O$, THF, $CH_3OH$; (iv) $R^1R^1$'NH, HATU, NMM, DMF; (v) arylboronic acid, $Pd(PPh_3)_4$, $K_3PO_4$, $Na_2CO_3$, $H_2O$, 1,4-dioxane, 90 °C, 12 h; (vi) DIPEA, HOBt, EDCI·HCl, *O*-(tetrahydro-2*H*-pyran-2-yl)hydroxylamine, $CH_2Cl_2$, DMF, rt, 12 h; (vii) 1M aq HCl, $CH_3CN$, MeOH, rt, 4 h.

crisis chronic myeloid leukemia (BC-CML) is a dire stage of CML, where patients are no longer responsive to treatment with BCR-ABL1 kinase inhibitors[23] such as imatinib, dasatinib, or nilotinib,[24,25] that in most cases ensure long-term survival to patients in chronic phase (CP) CML. BC-CML patients have high levels of nuclear β-catenin,[16,17,26] MNK1/2, eIF4E, and phosphorylated eIF4E[27,28] that are believed to promote not only resistance to treatment with BCR-ABL1 inhibitors, but also stimulate a proliferation of leukemic stems cells (LSCs)[16,29] via self-renewal.[30] Lim et al.[28] have shown that phospho-mimetic eIF4E (eIF4E-209D) elicits LSC self-renewal ability whereas the un-phosphorylatable eIF4E (eIF4E-209A) does not. They have, along with others, also shown that inhibition of β-catenin impairs the ability of primary BC-CML cells to self-renew to form colonies[16,26] and that the tumorigenic MNK/eIF4E/β-catenin axis plays an important role in BC-CML as well as in other cancers.[28,31,32]

The current best and only option to cure BC-CML is an allogenic bone marrow transplantation[33] (only beneficial to a small proportion of patients[33]), and consequently, long-term treatment of patients with BC-CML remains an unmet medical need.

Pharmacologic and knock-down inhibition of eIF4E phosphorylation by MNK1/2 prevents β-catenin activation[28,31,32] and suppresses the ability of LSCs to self-renew,[28] indicating that selective MNK1/2 kinase inhibition by a small molecule could be an avenue to treat patients with BC-CML. In addition, selective MNK1/2 kinase inhibition may be associated with minimal adverse effects, as *Mnk* knockout mice[2] are viable, healthy, and have normal hematopoiesis.



DOI: 10.1021/acs.jmedchem.7b01714
J. Med. Chem. 2018, 61, 4348−4369

**Scheme 3. Synthesis of Imidazopyrazine Analogues 36 and 37**[a]

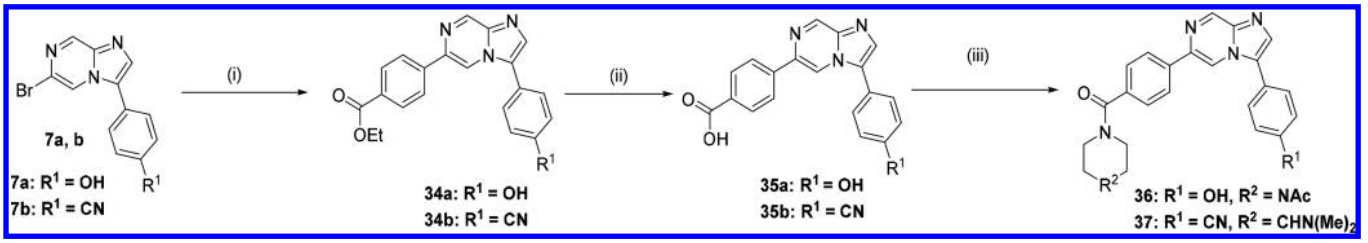


[a]Reagents and conditions: (i) (4-(ethoxycarbonyl)phenyl)boronic acid, $Pd(PPh_3)_4$, $Na_2CO_3$, $H_2O$, DMF, 90 °C, 12 h for **34a**, 2 h for **34b**; (ii) LiOH, THF, $CH_3OH$, rt, 5 h for **35a** and 12 h for **35b**; (iii) 1-(piperazin-1-yl)ethan-1-one or *N*,*N*-dimethylpiperidin-4-amine, HATU, NMM, DMF, rt, 3 h.

**Scheme 4. Synthesis of Imidazopyridazine Analogues 39, 40, 42, and 45**[a]

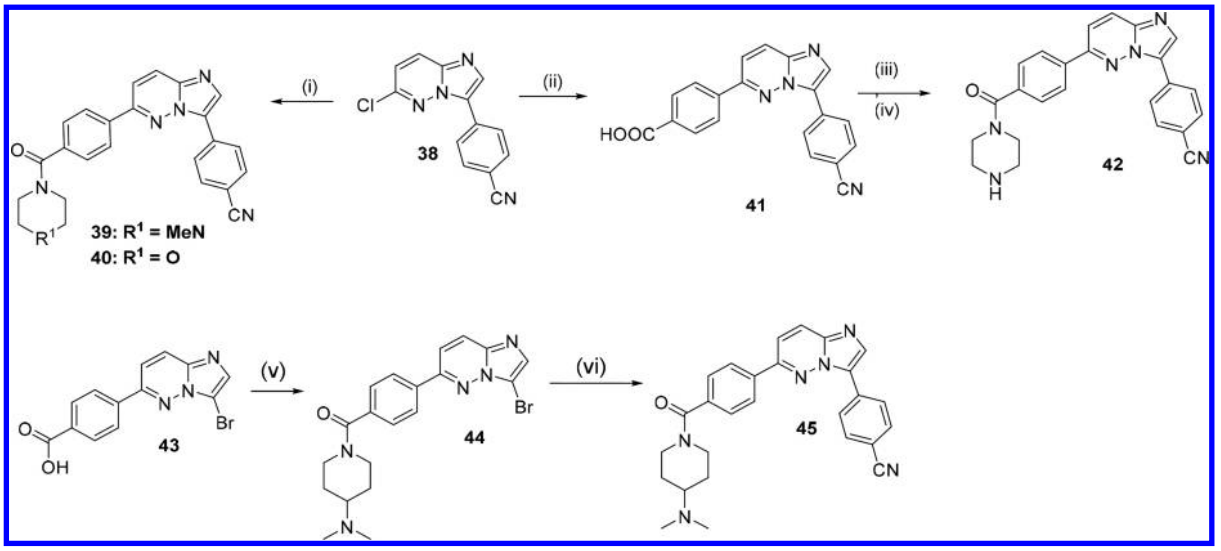


[a]Reagents and conditions: (i) (4-(4-methylpiperazine-1-carbonyl)phenyl)boronic acid, $Pd(PPh_3)_4$, toluene, EtOH, $K_2CO_3$, 140 °C, microwave reactor, 30 min; or morpholino(4-(4,4,5,5-tetramethyl-1,3,2-dioxaborolan-2-yl)phenyl)methanone, $Pd(dppf)_2Cl_2$, DMF, $H_2O$, $Cs_2CO_3$, microwave reactor, 140 °C, 30 min; (ii) 4-boronobenzoic acid, $Pd(dppf)_2Cl_2$, DMF, $H_2O$; $Cs_2CO_3$, 90 °C, 18 h; (iii) *tert*-butyl piperazine-1-carboxylate, HATU, NMM, DMF, rt, 18 h; (iv) TFA, $CH_2Cl_2$, rt; (v) *N*,*N*-dimethylpiperidin-4-amine, HATU, NMM, DMF; (vi) (4-cyanophenyl)boronic acid, $K_2CO_3$, $Pd(PPh_3)_4$, 1,4-dioxane, $H_2O$, 90 °C, 6 h.

Several inhibitors of MNK1/2 kinases have recently been reviewed,[34,35] notably CGP57380[36−38] and cercosporamide.[39] Both cercosporamide and CGP57380 lack kinase selectivity, and the latter is a weak MNK1/2 inhibitor with potency in the low micromolar range. Theodosia et al. have revealed MNK inhibitors with anti-proliferative activity against AML cell lines.[40,41] Likewise, merestinib, a nonselective MEK inhibitor, was also shown to inhibit MNK1/2 in AML progenitors with anti-leukemic effects.[42] The effectiveness of pharmacologic co-inhibition of MNKs and mTORC1 against BC-CML cells was recently published.[43,44] Han et al.[45] have disclosed potent MNK1/2 inhibitors but revealed no disease relevant biological data. Recently, two MNK inhibitors, BAY1143269 and eFT508, have progressed to clinical trial. BAY1143269,[46,47] a predominantly MNK1 inhibitor, was administered in a phase I clinical study to patients with advanced solid tumors.[48] eFT508, a potent and selective MNK1/2 inhibitor, is in phase II for the treatment of lymphoma, colorectal cancer, triple negative breast cancer, and hepatocellular carcinoma.[49−51]

To date there are little efficacy data and very few publications supporting the use of small-molecule MNK inhibitors to treat BC-CML. We have recently published our discovery efforts to generate a dual MNK and BCR-ABL1 inhibitor for the treatment of BC-CML[52] with a single agent, and we report herein a complementary approach with the design, synthesis, and structure−activity relationships of very selective MNK1/2 inhibitors. These compounds intentionally lack BCR-ABL1 inhibitory activity, and therefore can potentially be combined with the appropriate tyrosine kinase inhibitor for the treatment of BC-CML patients. Starting from fragments, small-molecule inhibitors of MNK1/2 were optimized, and a nominated preclinical development candidate was tested in a K562 mouse xenograft model.

## CHEMISTRY

The compounds described herein fall into three classes following the three central bicyclic rings explored, imidazopyrazine, imidazopyridazine, or imidazopyridine.

**Imidazopyrazines.** Compounds **4** and **5**, as shown in Scheme 1, were prepared in three steps starting from commercially available 6-bromoimidazo[1,2-*a*]pyrazine **1**, which was submitted to a copper mediated amination leading to 6-amide imidazopyrazines **2a**,**b**. The amide derivatives were brominated using NBS to give 3-bromo-6-amide imidazopyrazines **3a**,**b**, which were subjected to a Suzuki cross coupling reaction to afford **4** and **5**, respectively. Compound **8** was



DOI: 10.1021/acs.jmedchem.7b01714
J. Med. Chem. 2018, 61, 4348−4369

prepared in two successive Suzuki coupling steps, as depicted in Scheme 1, with 66% overall yield.

Imidazopyrazine analogues **19**–**33**, shown in Scheme 2, were prepared in a similar manner from **1**. Beginning with a Suzuki coupling to introduce a para-benzoyl ester at the imidazopyrazine 6-position to give **9**, which was halogenated at C-3 with either NBS or NIS to afford compounds **10** and **11**. The esters were hydrolyzed to carboxylic acids **12** and **13** that, in turn were converted to amides **14**–**18**. Arylation at C-3 using a second Suzuki cross coupling afforded **19**–**25** and **27**–**33**. Carboxylic acid **25** was converted into a protected hydroxamic acid intermediate, which was treated with an aqueous solution of hydrochloric acid to afford **26**.

Compounds **36** and **37** were synthesized in three steps comprising a Suzuki coupling, ester hydrolysis, and amide formation, as depicted in Scheme 3.

**Imidazopyridazines.** As illustrated in Scheme 4, compounds **39** and **40** were both prepared in one step from **38**. Compound **42** was synthesized in two steps starting with a Suzuki cross coupling between **38** and 4-boronobenzoic acid to give **41**, which was converted to amide **42**. Compound **45** was also prepared in two steps from commercially available acid **43**, which was converted to amide **44** followed by a Suzuki cross-coupling reaction to give **45**.

**Imidazopyridines.** The preparation of **47** and **48** is depicted in Scheme 5.

**Scheme 5. Synthesis of Imidazopyridine 47 and 48**[a]

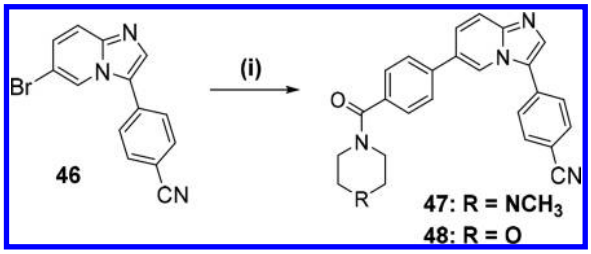


[a]Reagents and conditions: (i) (4-methylpiperazin-1-yl)(4-(4,4,5,5-tetramethyl-1,3,2-dioxaborolan-2-yl)phenyl)methanone, $(A\text{-}Phos)_2PdCl_2$, $NaHCO_3$, DMF, $H_2O$, 90 °C, 1 h; or morpholino(4-(4,4,5,5-tetramethyl-1,3,2-dioxaborolan-2-yl)phenyl)methanone, $Pd(PPh_3)_4$, $K_3PO_4$, 1,4-dioxane, $H_2O$, 90 °C, 19 h.

## RESULTS AND DISCUSSION

Fragment inhibitors of MNK1 published by Oyarzabal et al.[53] offered a diversity of scaffolds among which, a few imidazopyridazine analogues displayed high ligand efficiencies ranging from 0.32 to 0.52 kcal/mol per heavy atom. We found the imidazopyridazine scaffold to be an attractive starting point to generate novel inhibitors of MNK1/2 with drug-like properties, suitable for proof of concept in man. Accordingly, we gave it the highest priority.

Docking studies suggested that interactions with MNK1/2 could be improved by varying the bicyclic core and by modifying the substituents at C-3 and at C-6, whose alterations would considerably widen the structure–activity relationships (SAR) scope. Bicyclic cores were only selected, if modeling proposed a binding mode to the kinases similar to that of the imidazopyridazine. All these taken together suggested a need for SAR exploration of bicyclic analogues bearing substituents at both C-3 and C-6. Accordingly, our strategy was to divide this scaffold into three parts as outlined in Figure 1, where each part was investigated and the best of each were combined to give an optimized MNK1/2 inhibitor.

**Modeling.** We relied on molecular modeling to understand how our bicyclic-derived inhibitors interact with MNK1/2 and to guide optimization of their potency. A common structural feature in both MNK kinases is the DFD[54] motif, in which an aspartic acid Asp193 and Asp228 for MNK1 and MNK2, respectively, replaces the glycine of the DFG motif that is more common to kinases. A DFD-out structure of MNK1 (PDB ID: 2HW6)[55] is available, while MNK2 has been crystallized in both the DFD-in (PDB ID: 2HW7)[55] and DFD-out (PDB ID: 2AC3)[54] conformations. To validate our modeling, we searched the PDB for a co-crystal structure with inhibitors having the same scaffold. We found a structure (PDB ID: 4YMJ) of TRK kinase in the DFG-out conformation with a 4-(imidazo-pyridazin-3-yl)-benzonitrile inhibitor.[56] This compound has the same core as some of our inhibitors, and docking studies supported that it binds similarly to the TRK and MNK kinases. Consequently, we used the MNK DFD-out conformation in our modeling studies. The ATP binding sites of MNK1 and MNK2 share high sequence homology,[57] and modeling indicates that the compounds bind similarly to both kinases. Specifically, the bicyclic core acceptor nitrogen (N-1) hydrogen bonds with the amide backbone of the kinase hinge residues Leu127 in MNK1 and Met162 in MNK2. The C-3 substituents reside in the hydrophobic pocket formed by residues Phe124, Val63, Leu108, and Cys190 in MNK1 and the homologous residues Phe159, Val98, Leu143, and Cys225 in MNK2. The substituents at the core 6-position occupy the phosphate binding pocket close to the ATP ribose binding pocket. A major part of the inhibitor is buried inside the protein except for the substituents at the 6-position, which interact with the glycine-rich P-loop and the loop connecting the hinge region and helix αD of the C-terminal lobe. Compounds were docked into MNK1 and MNK2 using the automated docking program Glide 2017-3 release[58] using standard settings, and showed that top-ranked poses had the same binding mode as when manually modeled. The compounds described in this article interact mostly with the same amino acid residues in both MNK1 and MNK2. Furthermore, they inhibit both MNK1 and MNK2 with similar potency (less than 2-fold difference in all cases). In light of the similarities of the amino acids engaged in compound binding to MNK1/2 and the similarity between the inhibitory activities of the compounds against both MNK1 and MNK2,

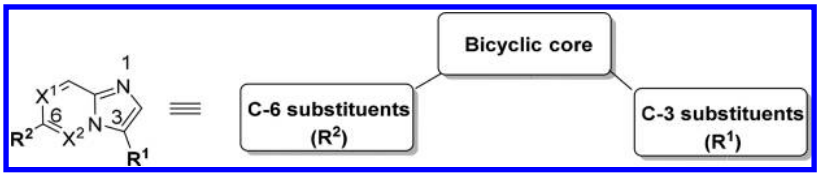


**Figure 1.** SAR exploration strategy.



DOI: 10.1021/acs.jmedchem.7b01714
J. Med. Chem. 2018, 61, 4348–4369

we will only discuss the modeling of inhibitors bound to MNK2.

The inhibitory activity of all compounds against MNK1/2 was assessed in a biochemical assay[52] with ATP at $K_m$ concentration of 1.2 mM and 250 $\mu$M for MNK1 and MNK2 assays, respectively. Compounds with a potency of 1 $\mu$M or lower against either MNK1 or MNK2, were assayed in a HeLa cell line[52] for their ability to inhibit the phosphorylation of eIF4E by MNK1/2. This functional assay relies on a sandwich immunoassay to quantify phosphorylated eIF4E. In both enzymatic and cell-based assays, each compound was tested in a dose-dependent manner, in duplicate, using eight points from a 3-fold serial dilution. $IC_{50}$ values were determined by nonlinear regression using GraphPad prism, and the values reported are the average of at least two experiments.

**C-6 Substituent Variation.** A quick probing of bicyclic scaffolds led to the imidazopyrazine derivatives shown in Table 1. The acetamide of **4** was replaced by a benzamide as in **5**

**Table 1. SAR of MNK1 and MNK2 Inhibitor Analogues 4, 5, 8, and 19**


| compd | $R_1$ | $IC_{50}$ ($\mu$M) MNK1[a] | MNK2[a] | HeLa[b] |
|---|---|---|---|---|
| **4** | AcNH | 0.789 | 0.515 | >2.5 |
| **5** | PhCONH | 3.35 | 1.08 | n.a. |
| **8** | Ph | 0.528 | 0.415 | 0.819 |
| **19** | 4-PhCONH$_2$ | 0.310 | 0.193 | 1.08 |

[a]*In vitro* assay where a compound's ability to inhibit MNK1 or MNK2 phosphorylation of a peptide substrate is determined as $IC_{50}$ values from the average of at least two measurements. [b]*In vitro* assay where a compound's ability to inhibit MNK1/2 phosphorylation of eIF4E on Ser209 and $IC_{50}$ values were determined as the average of at least two measurements. n.a. = not available.

which resulted in potency loss. The inhibitory activity toward MNK1/2 was restored by reversing the benzamide in **5** resulting in **19**. The primary amide function was removed to yield compound **8**, which was slightly less potent than compound **19**, suggesting that the amide of **19** contributes to potency.

Modeling of **4** (Table 1) into the ATP site of MNK2 shows that the imidazole N-1 hydrogen bond acceptor forms a hydrogen bond to the kinase hinge (Figure 2), very similar to that established by the N-1 of the adenine base of ATP. This is the backbone NH hydrogen bond donor of residues Leu127 in MNK1 and Met162 in MNK2. This hydrogen bond is stable during the molecular dynamics (MD) simulations (Supporting Information, MD file compound **4**). The 2-position of the imidazopyrazine is pointing toward the oxygen of the backbone carbonyl of Glu160, and the 8-position is pointing toward the oxygen of the backbone carbonyl of Met162.

Interactions between the aromatic hydrogen at the 2- and 8-positions and the backbone carbonyls are expected to be favorable to inhibitor binding[59] to the kinases. When either the 2- or 8-position is substituted all activity is lost (Supporting Information, Table S1).

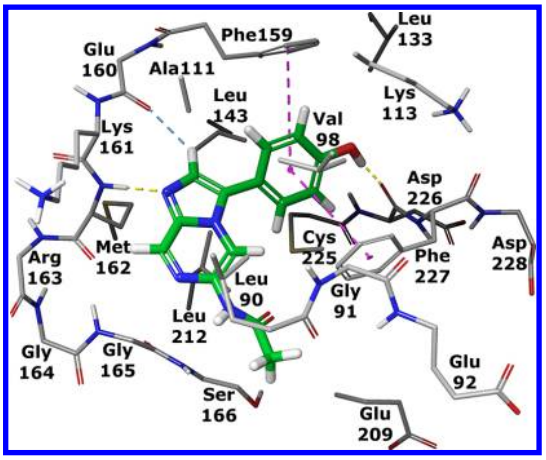


**Figure 2.** Compound **4** (Table 1) modeled into the MNK2 DFD-out X-ray structure (PDB ID: 2AC3). The binding site residues of MNK2 are shown in thin tube representation with gray carbon atoms. **4** is shown in thick tube with green carbon. Hydrogen bonds between MNK2 and **4** are shown with yellow dashed lines, $\pi-\pi$ interactions with magenta dashed lines, and aromatic hydrogen bond with blue dashed line.

The phenyl in the 3-position has extensive hydrophobic interactions with the kinase. It is sandwiched between the gatekeeper residue Phe159 and the DFD-motive residue Phe227 and engages in van der Waals contacts with the side chains of Val98, Ala111, Leu143, Cys225, and Leu212. The hydroxyl of **4** (Table 1) forms a stable hydrogen bond per MD simulations, with the backbone carbonyl of Asp226 from the DFD motif. The acetamide is solvent exposed on one side and binds in a largely hydrophobic area, where it interacts with the side chains of Leu90, Leu212, and Phe227. During the MD simulations, the nitrogen or carbonyl of the amide (**4**, **5**) periodically hydrogen bonds with the backbone NH or side chain of Ser166 either directly or water mediated. However, these interactions are not stable during the MD simulations and probably do not contribute much to the binding affinity.

The substitution of the methyl of acetamide (**4**) for a phenyl (**5**) led to a drop in potency, possibly due to a steric clash between the phenyl and Leu212 of the glycine-rich loop. Removing the amide linker favors a better interaction between the phenyl directly connected to C-6 (**8**, **19**) and residues Leu90, Leu212, and Phe227. Furthermore, the backbone NH of Ser166 is pointing toward the face of the phenyl resulting in an attractive electrostatic interaction between the negative $\pi$ cloud of the phenyl and the partial positive charge of the NH donor (Figure 3). These observations are in favor of the improvement in potency observed when a phenyl occupies the C-6 position. The amide of **19** marginally improved potency relatively to **8**, probably due to a hydrogen bond between the carbonyl and the side-chain hydroxyl of Ser166. Both compounds **8** and **19** inhibit eIF4E phosphorylation in cells with similar potencies, and **19** exhibited good permeability and favorable *in vitro* ADME properties, as shown in Table 2.

The primary amide of **19** was replaced by larger amides to yield *N*-methylpiperazine benzamide **20** and morpholine benzamide **32** (Table 3), both equipotent with **19**, but with improved permeability and solubility. The inhibitory activities of **19**, **20**, **32**, and **36** showed that the substituents represented by the $R^1$ equal to O, $NCH_3$, NAc (Table 3) had a moderate impact on inhibitory potency toward MNK1/2. Modeling (Figure 3) shows that the phenyl at 6-position makes van der


DOI: 10.1021/acs.jmedchem.7b01714
J. Med. Chem. 2018, 61, 4348−4369

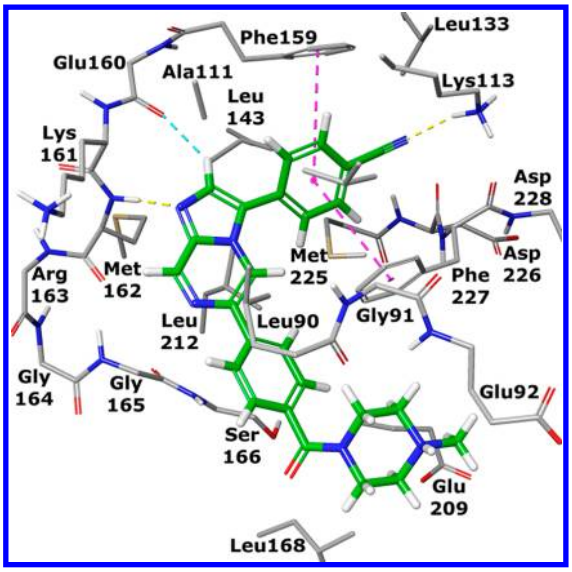


**Figure 3.** Compound **27** modeled into MNK2 DFD-out X-ray structure (PDB ID: 2AC3). The binding site residues of MNK2 are shown in thin tube representation with gray carbon atoms. **27** is shown in thick tube drawing with green carbons. Hydrogen bonds between MNK2 and **27** are shown with yellow dashed lines, $\pi-\pi$ interactions with magenta dashed lines, and aromatic hydrogen bond with blue dashed line.

**Table 2. Profile of Hit Compound 19**

| assay/property | value[a] |
|---|---|
| molecular weight (g/mol) | 330.35 |
| LogD(7.4)[b] | 2.03 |
| PAMPA ($\times 10^{-6}$ cm/s)[c] | 22.7 |
| HLM/MLM $T_{1/2}$ (min)[d] | 60/46 |
| Cyp 3A4/2D6 $IC_{50}$ ($\mu$M)[e] | >20/>20 |

[a]Average of at least two determinations, except for MW. [b]Distribution coefficient between 1-octanol and aqueous phosphate buffer at pH 7.4. [c]Parallel artificial membrane permeability assay at pH 7.4. [d]Half-life in human and mouse liver microsomes. [e]$IC_{50}$ for Cyp 3A4 and 2D6 inhibition.

Waals contacts with the side chains of Leu90, Leu212, Ser166 $\beta$-carbon, and Gly165 $\alpha$-carbon. In addition to the favorable interaction between the NH of Ser166 and the phenyl at C-6 described above, the piperazine substituent makes van der Waals contacts with the methylenes of Glu92 and Glu209. However, these residues are on the edge of the binding site and are solvated. Any interaction between the piperazine basic nitrogen and either acid is not likely to contribute much to the binding affinity. The methylpiperazine benzamide **20** and morpholine benzamide **32** amides appear to be the best overall C-6 substituents.

**C-3 Substituent Variation.** We next kept the methylpiperazine benzamide, our best solubilizing group, constant at C-6, and explored derivatization at C-3. Moieties such as pyridine derivatives, pyrimidine, bicyclic heterocycle, carbonyl bridged heterocycles failed to improve potencies relative to a phenyl substituent (Supporting Information, Table S2). These observations are in agreement with modeling studies, that support the hydrophobic nature of the binding site occupied by the phenyl at C-3. Consequently, our SAR investigations were then narrowed to only substituting the para position of phenyl at C-3. Removing the hydroxyl (**21**) or moving it to the ortho (**22**) or meta (**23**) positions resulted in a 5- to 30-fold loss in potency. The following para substituents illustrate how this part of the binding pocket can accommodate both hydrophobic and hydrophilic groups. The OH was replaced by $CH_3$ (**24**), COOH (**25**), CONHOH (**26**), CN (**27**), Cl (**28**), $CF_3$ (**29**), $CHF_2$ (**30**), and $CONH_2$ (**31**) and led to derivatives that inhibit MNK1 and MNK2 with potencies similar to that of **20**.

The hydroxamic acid derivative **26** showed a substantial improvement in potency relative to **20**, but **26** as well as the primary amide (**31**) and acid (**25**), all had poor permeability and consequently lacked cell-based activity. The carboxylic acid was replaced by a tetrazole (Supporting Information, Table S3) to give an equipotent compound, but with a bad permeability and practically no cell activity. The benzonitrile **27**, with a LogD of 1.67 (Table 3) is less lipophilic than analogues of similar potency (**28**, **29**, **30**) and displayed excellent solubility and permeability properties. Accordingly, the benzonitrile group was selected as the preferred substituent at C-3. At this stage, the improved compounds, exemplified by **27** and **33**, exhibited an imidazopyrazine with a benzonitrile at C-3 and methylpiperazine or morpholine benzamide at C-6.

MNK2 X-ray structures were examined to understand why the para position of the C-3 phenyl tolerates both hydrophobic and hydrophilic groups. Figure 2 represents **4** docked into MNK2 and shows that the para position is surrounded by hydrophobic residues Val98, side chain methylenes of Lys113, Phe227, and Phe159. Consequently, compounds with small hydrophobic para substituents like Me (**24**), Cl (**28**), $CF_3$ (**29**), and $CHF_2$ (**30**) have more hydrophobic interactions with the kinase than compound **21** the unsubstituted analogue. On the other hand, compounds with more polar substituents such as 4-OH (**20**), 4-$CO_2H$ (**25**), 4-CONHOH (**26**), 4-CN (**27**), and 4-$CONH_2$ (**31**) also have good inhibitory activity that could be the result of hydrogen bonding to the backbone carbonyl of Asp226 for hydrogen bond donating substituents (Figure 2) or with the basic side chain of Lys113 for acidic or hydrogen bond accepting groups as shown in Figure 3.

Modeling studies showed that the cyano group of **27** forms a hydrogen bond with Lys113, and during an MD simulation (Supporting Information, MD file compound **27**), this hydrogen bond was present for 60% of the time. The increased potency of **26** could be the result of two hydrogen bond interactions between the NH and OH of the hydroxamic acid group to Asp226 and Lys113, respectively.

**C-6 Substituent Variation.** We re-examined the suitability of benzamide moieties at C-6 to verify that the SAR established with the C-3 phenol derivatives holds true for the C-3 benzonitrile analogues. Accordingly, two benzonitrile derivatives, morpholino (**33**) and *N,N*-dimethylamino piperidinyl (**37**) were generated. **27** and **33** are equipotent toward MNK1/2 inhibition, just as the phenolic derivatives **20** and **32** are. Analogues **27**, **33**, and **37** were all of similar potency toward MNK1 inhibition, but for MNK2, **37** is 3- and 4-fold more potent than **27** and **33**, respectively.

Compounds **27**, **33**, and **37** were found to have favorable ADME properties as shown in Table 4. They were administered orally to mice, and **27**, with a bioavailability of 48%, was the fastest absorbed, with a $C_{max}$ and AUC 4−6 times higher than those of **33** and **37** (Supporting Information, Table S4). Compound **27** achieves an excellent selectivity and inhibits only four kinases at more than 50% out of 104 kinases when tested at a concentration of 10 $\mu$M (Supporting Information, Table S5). Overall, **27**, combines excellent physicochemical


DOI: 10.1021/acs.jmedchem.7b01714
J. Med. Chem. 2018, 61, 4348−4369

Table 3. SAR of Imidazopyrazine Derivatives 20−33, 36, and 37 and Their Physicochemical Properties

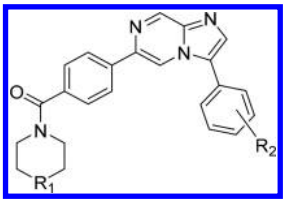

| compd | $R_1$ | $R_2$ | $IC_{50}$ ($\mu$M) MNK1[a] | $IC_{50}$ ($\mu$M) MNK2[a] | $IC_{50}$ ($\mu$M) HeLa[b] | LogD(7.4) | PAMPA ($\times10^{-6}$ cm/s) | solubility ($\mu$g/mL) |
|---|---|---|---|---|---|---|---|---|
| **20** | $NCH_3$ | 4-OH | 0.284 | 0.140 | 0.189 | 2.25 | 34.7 | 114 |
| **21** | $NCH_3$ | H | 2.68 | 1.43 | 1.92 | n.a. | n.a. | n.a. |
| **22** | $NCH_3$ | 2-OH | 9.50 | 5.17 | n.a. | n.a. | n.a. | n.a. |
| **23** | $NCH_3$ | 3-OH | 1.30 | 0.742 | 1.33 | 2.31 | 33.2 | 116 |
| **24** | $NCH_3$ | 4-$CH_3$ | 0.600 | 0.410 | 1.21 | n.a. | n.a. | n.a. |
| **25** | $NCH_3$ | 4-$CO_2H$ | 0.700 | 0.355 | >2.5 | −1.37 | 0.10 | >22 |
| **26** | $NCH_3$ | 4-CONH(OH) | 0.060 | 0.031 | >2.5 | n.a. | n.a. | n.a. |
| **27** | $NCH_3$ | 4-CN | 0.499 | 0.502 | 0.440 | 1.67 | 102 | >125 |
| **28** | $NCH_3$ | 4-Cl | 0.331 | 0.217 | 0.759 | 2.96 | 71.3 | 118 |
| **29** | $NCH_3$ | 4-$CF_3$ | 0.574 | 0.389 | 1.99 | 2.95 | 87.4 | 90.4 |
| **30** | $NCH_3$ | 4-$CHF_2$ | 0.369 | 0.336 | 1.63 | 2.55 | 76.2 | 66.9 |
| **31** | $NCH_3$ | 4-$CONH_2$ | 0.294 | 0.187 | >2.5 | 0.98 | 1.78 | 126 |
| **32** | O | 4-OH | 0.125 | 0.113 | 0.130 | 2.21 | 50.2 | 11.5 |
| **33** | O | 4-CN | 0.570 | 0.454 | 0.748 | 1.77 | 43.1 | 11.1 |
| **36** | $NCOCH_3$ | 4-OH | 0.224 | 0.160 | >2.5 | 1.68 | 2.82 | 144 |
| **37** | $CHN(CH_3)_2$ | 4-CN | 0.238 | 0.143 | 0.640 | 0.73 | 64.7 | >45 |

[a]*In vitro* $IC_{50}$ against MNK1 and MNK2; average of at least two determinations. [b]eIF4E phosphorylation inhibition measured using HeLa cell line, average of at least two determinations. n.a. = not available.

Table 4. Microsomal Stability, Cyp Inhibition, Permeability, and Plasma Protein Binding (PPB) Properties of Selected Compounds

| compd | $T_{1/2}$ (min)[a] HLM/MLM | $T_{1/2}$ (min)[a] RLM/DLM | Cyp 3A4/2D6 $IC_{50}$ ($\mu$M) | Caco-2 Papp A-B[b] | Caco-2 efflux ratio | PPB (%) human | PPB (%) mouse |
|---|---|---|---|---|---|---|---|
| **27** | 41/37 | n.a. | >20/>20 | 6.87 | 5.6 | 98.4 | 87.1 |
| **33** | >60/>60 | n.a. | >20/>20 | 17.9 | 1.73 | n.a. | n.a. |
| **37** | >60/>60 | n.a. | >20/>20 | 1.14 | 7.57 | n.a. | n.a. |
| **39** | 17/23 | n.a. | >20/>20 | 14.6 | 4.84 | 99.9 | 95.9 |
| **40** | 53/>60 | >60/>60 | >20/>20 | 38.5 | 0.64 | 99.9 | 94.5 |
| **42** | >60/42 | n.a. | 5.6/n.a. | 1.13 | 29.9 | n.a. | n.a. |
| **45** | 47/>60 | n.a. | n.a. | 3.00 | 13.27 | n.a. | n.a. |
| **47** | 20/11 | n.a. | 3.9/>20 | 5.43 | 4.84 | 99.7 | 90.33 |
| **48** | 48/56 | >60/>60 | >20/>20 | 30.50 | 1.42 | 99.7 | 84.2 |

[a]HLM/MLM, metabolic stability measured in human and mouse liver microsomes; RLM/DLM, metabolic stability determined in rat and dog liver microsomes. [b]Papp in $10^{-6}$ cm/s. n.a. = not available.

properties (Table 3) with good *in vitro* and *in vivo* ADME properties and excellent PK properties and kinase selectivity profile. Thus, compound **27** was selected as the lead compound for the lead optimization phase.

**Multiparameter Lead Optimization.** *Increasing Potency: Swapping Cores.* Alteration at C-3 and C-6 of the imidazopyrazine core produced **27** with an inhibitory potency of 0.5 $\mu$M against MNK1 and MNK2, in both enzymatic and cellular assays. At this stage, the core is the only part of the scaffold that was not modified, and we thought that its alterations could modulate potency and/or ADME properties as done by others.[60−62]

Accordingly, in addition to imidazopyrazine, six bicyclic rings were investigated (Table 5 and Supporting Information, Table S6). Modeling studies have shown that their binding mode to MNK1/2 remain similar to that of imidazopyrazine analogues; all derived analogues have in common the N-1 binding to hinge Ser166 and the CN hydrogen bonding to Lys223, and exhibited previously described hydrophobic interactions for phenyl groups at both C-3 and C-6.

Briefly, in comparison to the imidazopyrazine **27**, [1,2-*a*]pyrimidine and 1*H*-imidazo[4,5-*c*]pyridine analogue (Supporting Information, Table S6) were less potent, and 1*H*-benzo[*d*]imidazole derivative (Supporting Information, Table S6) was equipotent to **27**. In contrast, the pyrazolo[1,5-*a*]pyrimidine analogue was 10-fold more potent than **27** (Supporting Information, Table S6), and compounds from pyrazolo[1,5-*a*]pyrimidine series showed SAR, physicochemical, and PK properties similar to those of the imidazopyridazine analogues. Therefore, we focused on the imidazopyrazine, imidazopyridazine, and imidazopyridine cores, and derived analogues as shown in Table 5.



DOI: 10.1021/acs.jmedchem.7b01714
J. Med. Chem. 2018, 61, 4348−4369

Table 5. Influence of the Bicyclic Core on Potency: From Imidazopyrazine to Imidazopyridazine and Imidazopyridine

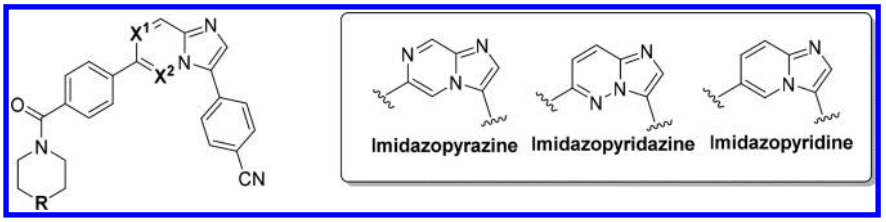


| compd | $X^1$ | $X^2$ | R | $IC_{50}$ ($\mu$M) MNK1[a] | MNK2[a] | HeLa[b] | PAMPA ($\times 10^{-6}$ cm/s) | LogD7.4 | solubility ($\mu$g/mL) |
|---|---|---|---|---|---|---|---|---|---|
| **27**[c] | N | CH | $NCH_3$ | 0.499 | 0.502 | 0.440 | 102 | 1.67 | >125 |
| **39** | CH | N | $NCH_3$ | 0.020 | 0.025 | 0.326 | 25.0 | 2.82 | 86.0 |
| **40** | CH | N | O | 0.023 | 0.041 | 0.421 | 30.0 | 2.10 | 1.80 |
| **42** | CH | N | NH | 0.016 | 0.026 | 0.220 | 45.8 | 2.00 | 115 |
| **45** | CH | N | $CHN(CH_3)_2$ | 0.009 | 0.011 | 0.431 | 75.3 | 2.19 | 148 |
| **47** | CH | CH | $NCH_3$ | 0.084 | 0.072 | 0.229 | 81.9 | 2.48 | 137 |
| **48** | CH | CH | O | 0.064 | 0.086 | 0.321 | 74.4 | 2.61 | 55.4 |

[a] *In vitro* $IC_{50}$ against MNK1 and MNK2. [b] eIF4E phosphorylation inhibition measured using HeLa cell line. [c] **27** was shown to illustrate the bicycle ring influence on potency in one table. $IC_{50}$'s are the average of at least two determinations.

Similarly, imidazopyridazine analogues **39**, **40**, and **42** are more potent than imidazopyrazine analogues **27** and **33**. This trend is also observed when the imidazopyrazine core is replaced by an imidazopyridine with an improvement in potency, of 6- to 9-fold for MNK1 and of 5- to 7-fold for MNK2, seen when comparing imidazopyrazines **27** and **33** to imidazopyridines **47** and **48**.

In HeLa cells, inhibitory data of eIF4E phosphorylation shown in Table 5 are clustered between 0.22 and 0.44 $\mu$M. This inhibition is often weaker by 3- to 47-fold in whole-cell as compared to cell-free assays, probably due to permeability issues (**39**, **40**, **42**), nonspecific binding or a combination of both. Highly permeable compounds (**27**, **47**, **48**) exhibit a smaller potency difference between enzymatic and cellular data, and **27**, the most permeable compound, is equally potent in both assays. Compound **45** is 47-fold less potent in cellular assays despite a good PAMPA permeability. However, **45** has a high Caco-2 efflux ratio of 13 (Table 4) that could explain the loss of potency.

To rationalize the impact of N-7 on potency, we examined the structural models which revealed that the imidazopyrazine N-7 (Figures 2 and 3) is not involved in any hydrogen bond in any of the docked complexes studied. On the contrary, it resides in a hydrophobic environment and has van der Waals interactions with Gly165 $\alpha$ carbon and Leu90 side chain, as visualized in Figures 2 and 3. This may account for part of the approximately 5- to 10-fold gain in potency observed when this N-7 nitrogen is replaced by a CH (compare **33** to **48**). Indeed, our previous modeling studies[63] have also shown the important contribution of hydrophobic interactions to the potency of the compounds.

It may be surprising that compounds with an imidazopyridazine scaffold were also substantially more potent than the imidazopyrazine analogues as both cores have two nitrogen atoms with a lone pair that can be solvated. The N-5 of the imidazopyridazine is also surrounded by hydrophobic residues (Leu90 and Leu212). We believe that the difference in exposure of the lone pairs plays a determining role in the influence of the core on potency. In the imidazopyrazines the lone pair is shielded by the C-6 phenyl where as in the imidazopyridazines the lone pair is shielded by both the C-3 and C-6 phenyls. This impacted the interaction between the ligand and protein as well as the solvation energy.

DFT calculations indicate that the desolvation penalty for the imidazopyrazine N-7 may be much higher than that of the imidazopyridazine N-5, and it costs 10.8 kJ/mol more to remove the water from the imidazopyrazine complex in Figure 4.

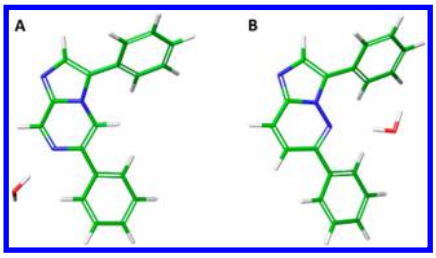


**Figure 4.** A single water molecule was placed in front of the imidazopyrazine N-7 (A) and imidazopyridazine N-5 (B). The complexes were minimized using DFT-B3LYP 6-31G**.

In contrast to the benzamide's minor influence on binding in imidazopyrazine series, the 4-*N*,*N*-dimethylamino piperidine **45** in the imidazopyridazine series is substantially more potent than piperazine and morpholine benzamide analogues **39** and **40**, respectively.

The piperidine-dimethylamine (**45**) in Figure 5 is sandwiched between hydrophobic residues Gly91, Leu168, and Phe227, while the base may interact with the acids Glu92 and Glu209. Figure 5 shows the interactions of the dimethylamino piperidine group **45** with Glu209 and Phe227 of MNK2. In the MD simulations, the basic nitrogen interacts with the side chain of Glu209 during most of the simulation. However, when bound to MNK2, this part of the inhibitor is solvent exposed; solvent effects are likely to shield the contributions of any electrostatic interactions, and they may not contribute much to the binding affinity.

We speculate that the *N*,*N*-dimethylamino piperidine interacts better with Phe227 and Glu209 than the *N*-methylpiperazine. During the MD simulations (Supporting Information, MD file compound **45**), the interactions with



DOI: 10.1021/acs.jmedchem.7b01714
J. Med. Chem. 2018, 61, 4348−4369

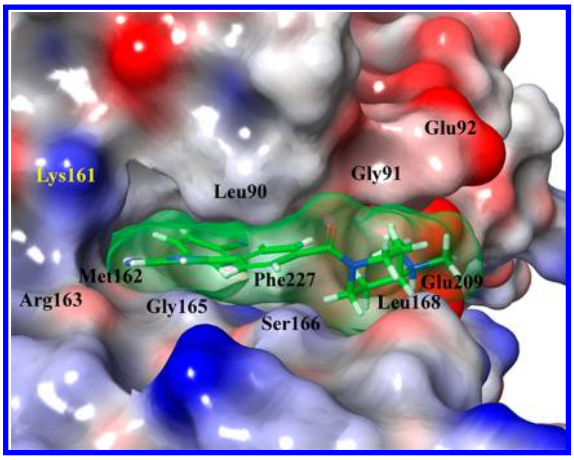


**Figure 5.** Compound **45** docked into MNK2 catalytic site. MNK2 is shown as an electrostatic surface. The inhibitors are shown in stick with green carbon and a transparent green surface.

these residues were stable for **45** while they were only observed during 50% of the simulations for **20**.

**ADME and PK.** *Modulation of ADME Properties: Correcting Issues Related to N-Alkylated Benzamides.* A selection of compounds, shown in Table 4, were evaluated *in vitro* to assess their metabolic stability, Cyp inhibition, and protein binding properties. It appears that substituting the imidazopyrazine core effectively led to more potent derivatives **39** and **47** (Table 5), but with an increased metabolic liability (Table 4). Methylpiperazine **39** and **47** are unstable in human and mouse liver microsomes, and this is most likely attributable to *N*-demethylation. To address that issue morpholine **40**, piperazine **42**, and *N,N*-dimethylamino piperidine **45** derivatives were generated and were found to be metabolically stable. Unfortunately, both piperazine **42** and dimethylamino piperidine **45** derivatives were subject to a high efflux ratio (Table 4) which might negatively impact their PK properties. Morpholine derivatives **40** and **48** showed low metabolic liability in mouse, rat, dog, and human microsomes, and low Cyp 3A4 and 2D6 inhibition, and they exhibited a higher cell permeability as per the Caco-2 assay (Table 4) compared to the basic piperazine and piperidine analogues.

*Pharmacokinetic Properties.* In spite of the high efflux ratio of **45**, it was orally administered to mice at 5 mg/kg and gave a poor systemic exposure with a $C_{max}$ of 69 ng/mL and an $AUC_{0\text{-}inf}$ of 347 ng·h/mL. In contrast, **40** and **48** exhibited higher exposure and substantially improved PK properties relative to the lead **27** when comparing AUC and $C_{max}$ values (Table 6). Indeed, compared to **27**, compounds **40** and **48** exhibited several characteristics favorable to good exposure, including lower basicity, higher Caco-2 permeability, and a lower Caco-2 efflux ratio.

*Kinase Selectivity.* Compounds **40** and **48** were tested against a panel of 104 kinases together with representative MNK inhibitors such as CGP57380,[36−38] cercosporamide,[39] and AST-487.[52,64] These known MNK inhibitors are often used in biological studies but their selectivity profiles were not readily available. CGP57380 is a multikinase inhibitor[65] as it was found to inhibit ABL1 (E255 K), ABL1 (WT), MEK1, MEK2, MNK1, MNK2, and RET at more than 99% (Supporting Information, Table S5).

Table 7 shows that **40** and **48** are selective, and specifically, imidazopyridine **48** inhibits only two kinases at ≥65%, six

**Table 6. Mouse Pharmacokinetics Data for Compounds 40 and 48**

| | 40 | | 48 | |
|---|---|---|---|---|
| dose (mg/kg) | 1 | 5 | 1 | 5 |
| route of administration | i.v. | p.o. | i.v. | p.o. |
| $C_0$ (ng/mL) | 2940 | | 2379 | |
| $C_{max}$ (ng/mL) | | 4405 | | 2481 |
| $T_{max}$ (h) | | 0.5 | | 0.5 |
| $T_{1/2}$ (h) | 2.32 | 2.14 | 1.7 | 1.77 |
| CL* (L/h/kg) | 0.16 | | 0.56 | |
| $AUC_{0\text{-}t}$ (last) (ng·h/mL) | 6124 | 24093 | 1761 | 5484 |
| *F* (%)[a] | 79 | | 64 | |

[a]*F* (%) calculated after i.v. and p.o. administration at 1 mg/kg and 5 mg/kg respectively of **40** and **48**. Formulations: p.o., 0.5% MC + 0.1% TW80 + sterile MQ water; i.v., 10% NMP + 40% PEG300 + sterile MQ water, 10% Cremophor + 10% DMA + sterile MQ water.

kinases fewer than imidazopyridazine **40**. The bicyclic core of **48** had an unexpected influence on its kinase selectivity, and the difference in the torsion between the bicyclic ring and the phenyl at C-3 could be a plausible explanation of why **48** is more selective than **40**. There is a 29° versus 42° torsion variation in DFT-B3LYP 6-31** minimized structures. The more coplanar **40** probably has a shape that allows it to fit better to a greater number of kinases.

*Cell-Based Anti-proliferative Activity.* The anti-proliferative effects of **40** and **48** were assessed *in vitro*, using CellTiter-Glo viability assay against 25 hematological cancer cell lines including the K562 cell line that overexpresses eIF4E (K562 o/e eIF4E)[28] (Supporting Information, Table S7). The $IC_{50}$'s were in general in the micromolar range similar to published data.[34,43,45,66] Compound **40** appears to be more potent than **48** with submicromolar $IC_{50}$, especially against GK-5, DOHH2, AHH-1, and P3HR-1 cell lines. We speculate that the superior activity of **40** against these cell lines could be the result of the combination of its potency and off-target inhibition of kinases such as PDGFRA and FLT3, against which **40** gave an inhibitory potency of 0.25 and 0.88 μM, respectively. MNK1/2 inhibitors that show strong anti-proliferative effects *in vitro* have been known to often inhibit other kinases.[34,39]

In contrast, **40** and **48** alone or in combination with imatinib or dasatinib were both able to suppress the ability of leukemic stem cells from BC-CML patient to form colony (data to be published elsewhere). This was previously described for nonselective MNK1/2 inhibitors AST-487, CGP57380, and cercosporamide, and it was shown that imatinib and dasatinib alone do not inhibit the self-renewal activity of LSCs.[28]

*Selection of Compound 48 as a Preclinical Candidate.* A comparison of the two optimized compounds, **40** and **48**, shows that **40** is the most potent in the enzymatic assay, but that potency did not carry over to eIF4E phosphorylation inhibition in HeLa cells, where **48** is slightly more potent. Compound **48** has a greater solubility, permeability and an excellent kinase selectivity. In maximum tolerated dose studies, oral administration of **48**, showed no weight loss and no clinical adverse effects in healthy mice up to the tested dose of 200 mg/kg.

To avoid any ambiguities in interpreting efficacy studies, a compound which inhibits fewer kinases will be preferred for investigating the impact of the inhibition of MNK1/2 on biological processes. In light of these data, compound **48** was ranked higher and was selected as the preclinical candidate.


DOI: 10.1021/acs.jmedchem.7b01714
J. Med. Chem. 2018, 61, 4348−4369

Table 7. Kinase Selectivity Profile of 40 and 48 Screened against a Panel of 104 Kinases at 1 $\mu$M[a]

| Compounds | | 40 | 48 |
|---|---|---|---|
| TREEspots | | 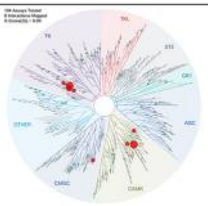 | 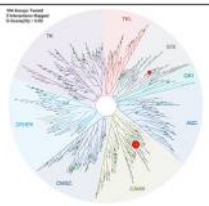 |
| Number of Kinases inhibited* | >65% | 8 (DRAK1; FLT3; KIT; MNK2; PDGFRA; PDGFRB; PHKG2; SRPK3) | 2 (MEK; MNK2) |
| | >90% | 3 (FLT3; MNK2; PDGFRB) | 1 (MNK2) |

[a]Kinase inhibition data are from a competition assay with a proprietary ligand to determine the compound's binding affinity against a panel of 104 kinases.

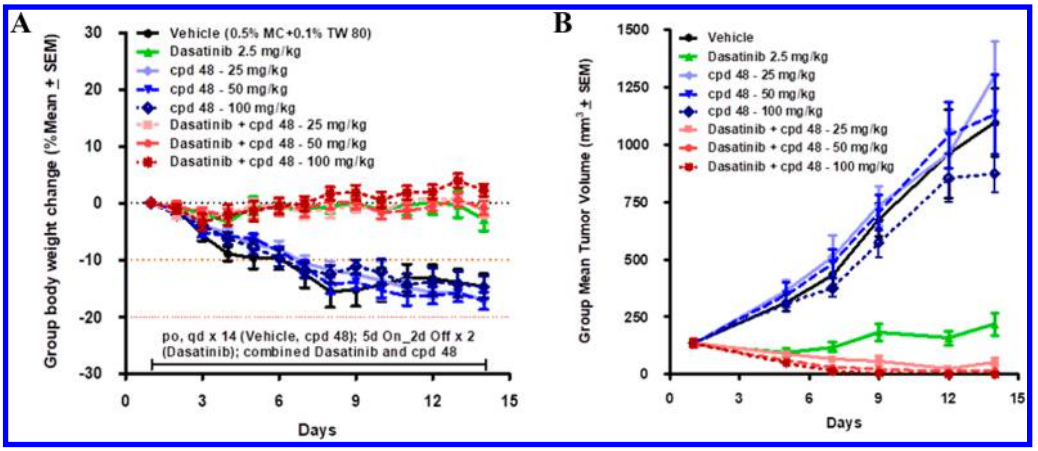


**Figure 6.** Antitumor efficacy of **48** after oral administration alone or in combination with dasatinib to K562 o/e eIF4E SCID mouse xenograft model with eight mice per group. (A) Mouse body weights expressed as (mean ± SEM). (B) Tumor growth rates expressed as volumes (mean ± SEM).

*In Vivo Efficacy.* We have reported that dual specific MNK1/2 and BCR-ABL1 inhibitors potently inhibited the proliferation of five BC-CML lines *in vitro*, and these inhibitors elicited a dose-dependent anti-tumor activity in an *in vivo* mouse xenograft model.[52] As MNK1/2 and BCR-ABL1 inhibitory activities were combined into one molecule, it was challenging to distinguish the contribution of MNK1/2 inhibition in the observed biological response. Now, we have shown that selective MNK1/2 inhibitors **40** and **48** are much less anti-proliferative against the five BC-CML cell lines (Supporting Information, Table S7). However, there are emerging data[67−69] that support that MNK1/2 inhibition effect *in vivo* could be greatly enhanced by the tumor microenvironment or the stroma without which, the amplitude of MNK1/2 inhibitors anti-proliferative effect on BC-CML cell lines in *in vitro* cellular assays could appear to be much weaker. Accordingly, compound **48** was selected for further evaluation *in vivo* in a mouse xenograft model. The antitumor effect of compound **48** was then assessed in a K562 e/o eIF4E mouse xenograft model after oral administration at 25, 50, or 100 mg/kg alone or in combination with a 2.5 mg/kg fixed dose of dasatinib throughout the study (Figure 6).

Figure 6A shows that the treatment was well tolerated, and the weight loss observed with the vehicle or compound **48** administered alone is due to the burden of the tumor growth on mice.

Dasatinib at 2.5 mg/kg elicited a tumor growth inhibition (TGI) of 88% (Figure 6B) with one tumor-free animal. In contrast, **48** alone only yields a maximum TGI of 23% at the highest administered dose of 100 mg/kg, which did not impede tumor growth, and was similar to the nontreated animals. Combining **48** with 2.5 mg/kg of dasatinib not only increased tumor growth inhibition in a dose-dependent manner but, more importantly led to 2, 5, and 8 out of 8 tumor-free animals at 25, 50, and 100 mg/kg, respectively (Supporting Information, Table S8). The combination of **48** and dasatinib inhibited tumor growth at all tested doses, and no weight loss was recorded (Figure 6A). Both the combination of **48** and dasatinib and, on the other hand, the dual MNK1/2 and BCR-ABL1 inhibitors[52] prevented tumor growth in the same mouse xenograft model. The combination study clearly showed, that a


DOI: 10.1021/acs.jmedchem.7b01714
J. Med. Chem. 2018, 61, 4348−4369

selective MNK1/2 inhibitor plays a role in TGI by enhancing the antitumor effect of dasatinib.

*Biomarker Study.* Western blot analysis of tumor samples excised from mice administered with 2.5 mg/kg of dasatinib and 100 mg/kg of **48** (Supporting Information Figure S1) revealed a maximum reduction in phosphorylated CRKL, a BCR-ABL1 substrate, from 4 to 8 h post dose. The reduction of phosphorylated eIF4e was significant after 1 h post dose and was sustained at 4 and 8 h post dose. These observations are consistent with the tumor growth inhibition induced by the combination of **48** and dasatinib and shows that both MNK1/2 and BCR-ABL1 kinases are inhibited *in vivo*.

## CONCLUSION

Starting from bicyclic fragment hits, selective and potent MNK1/2 inhibitors were designed and synthesized. Substituents at both C-3 and C-6 and the bicyclic moiety were optimized. The imidazopyridazine and imidazopyridine derivatives, which required a nonbasic benzamide for optimal PK properties, also showed that these cores were equally effective at increasing potency for MNK1/2 inhibition and at modulating kinase selectivity profiles. Imidazopyridine derivative **48** displayed excellent kinase selectivity and significantly enhanced the anti-tumor activity of dasatinib in a BC-CML mouse xenograft model. This is in agreement with our previous anti-tumor data obtained with single compound dual MNK/BCR-ABL1 inhibitors, for which the impact of MNK inhibition could not be clearly established. Biomarker studies show that the combination effectively reduced the ability of both MNK1/2 and BCR-ABL1 kinases to phosphorylate their substrates eIF4E and CRKL, respectively. Treatment of patients resistant to dasatinib with a combination of MNK1/2 inhibitor and dasatinib should overcome the MNK-eIF4E axis-mediated resistance and restore sensitivity to dasatanib treatment. In addition, the combination might require a lower dose of dasatinib to achieve efficacy, alleviating dasatinib toxicity. This combination therapy with MNK1/2 inhibitors could be extended not only to other BCR-ABL1 inhibitors current or future, but also to other therapies using kinase inhibitors that have become ineffective due to an overexpression of phosphorylated eIF4E.

Compound **48** is currently in phase 1 clinical trial, where its benefit to BC-CML patients treated with dasatinib is being evaluated.

## EXPERIMENTAL SECTION

**Molecular Modeling.** The apo DFG-out MNK1 and MNK2 X-ray structure PDB entries 2HW6[55] and 2AC3,[54] respectively, were downloaded from the Protein Data Bank[70] and prepared with the protein preparation wizard in Maestro 2017-3 release[58] using standard settings. This included the addition of hydrogen atoms, bond assignments, removal of water molecules farther than 5 Å from the ligand, protonation state assignment, optimization of the hydrogen bond network, and restrained minimization using the OPLS3 force field.[71] The missing loops were added to the 2AC3 structure, these were adopted from a previously published model.[63] The inhibitors were built using Maestro and minimized using MacroModel 2017-3 release[58] before being manually docked into the MNK2 ATP-binding site. The inhibitor−protein complex was finally minimized using Macromodel. All residues more than 9 Å from the ligand were constrained before the complex was subjected to 500 steps of Polak−Ribiere conjugate-gradient[72] minimization using the OPLS3 force field[71] and the GB/SA continuum solvation method.[58]

The protein complexes were then subjected to 250 ns of unconstrained MD simulation using Desmond 4.8.[58] The system for MD was build using the System Builder in Desmond. The protein−inhibitor complex was placed in an orthorhombic box with a 10 Å buffer in an orientation that minimized total box volume. The SPC explicit solvent model using water as solvent was employed. The system was neutralized by adding $Na^+$ ions, and the NaCl salt concentration was set to 0.15M. Under an NPT ensemble class with $T$ = 300 K, $P$ = 1.01325 bar, with the system relaxed MD simulations were carried out for 250 ns. Analyses of secondary structure, RMSF, and ligand−protein interactions were performed using the Simulation Interactions Diagram tool in Desmond (Supporting Information, MD files for compounds **4**, **27** and **45**). The binding orientation and ligand−protein interactions shown in Figures 2, 3, and 5 are representative of the interactions observed during the MD simulation.

The model systems in Figure 4 were built in Maestro and minimized using the DFT-B3LYP with the 6-31G** basis set in Jaguar 2017-3 release.[58] The water interaction energy was calculated by subtracting the gas-phase energy of the free water and inhibitor from the energy of the complex.

**General Chemistry.** Reagents were purchased from commercial sources and were used as received.

$^1$H NMR spectra were recorded on a Bruker AVANCE 400 spectrometer at 400 MHz or Bruker AVANCE 300 spectrometer at 300 MHz with the solvent as reference. Samples were prepared as solutions in a deuterated solvent and referenced to the appropriate internal nondeuterated solvent peak. The following abbreviations were used to explain the multiplicities: s = singlet, d = doublet, t = triplet, q = quartet, quint = quintet, m = multiplet, pent = pentet, hex = hextet, b = broad. $^{13}$C NMR spectra were recorded at 100 and 125 MHz using an internal deuterium lock.

LC MS analyses were performed on a Agilent 1200 series with PDA detector and ion trap mass detector; Waters Acquity UPLC with PDA, ELSD, and Quattro micro mass detector; Waters Acquity UPLC with PDA and 3100 mass detector; Agilent 1100 and 1200 series with PDA detector and single quadrupole mass detector; and Shimadzu 2020 with PDA detector and single quadrupole mass detector. Electrospray-ionization time-of-flight high-resolution mass spectrometry (ESI-TOF-HRMS) was conducted on an Agilent 6210 ESI-TOF (Agilent Technologies). MS (ESI) were recorded on an Agilent 6120 Quadrupole LC/MS system.

Reverse-phase HPLC analyses were performed on a Waters Alliance HPLC system with a PDA detector, Waters Acquity UPLC system with a PDA detector; Varian prostar system with PDA detector. The following columns were used: Waters Acquity BEH C18, 100 × 2.1 mm, 1.7 μm; Waters X-Bridge C18, 250 × 4.6 mm, 5 μm; Waters X-Bridge C8, 250 × 4.6 mm, 5 μm; Waters X-Bridge C18, 100 × 4.6 mm, 3.5 μm; Phenomenex Luna C18, 100 × 4.6 mm, 5 μm; and Phenomenex Luna C18, 250 × 4.6 mm, 5 μm. Purifications by preparative HPLC were performed on a Waters 2545 Binary Gradient prep system with 2767 Auto sampler, Gilson GX-281 with UV detector, Shimadzu Prominence UFLC with diode array; Shimadzu Prominence with UV detector; Varian Prostar with PDA detector. All reagents and solvents were commercial grade and were used as received unless noted otherwise.

Flash chromatography was performed using a Teledyne Isco RF200 or on a Biotage SP1 combiflash purification, both systems using using prepacked silica gel columns. Thin-layer chromatography (TLC) was performed using EMD TLC silica-gel 60$F_{254}$ plates. Visualization of TLC plates was performed using UV light (254 nm). Melting points were determined by the capillary method on a Stuart SMP30 apparatus and are uncorrected.

The purity values for all biologically tested compounds were found to be greater than or equal to 95% determined from HPLC analyses.

**General Synthetic Procedures.** *General Procedure A: Aromatic Halogenation.* A solution of bicyclic derivative (*N*-(imidazo[1,2-*a*]pyrazin-6-yl)acetamide) and *N*-bromosuccinimide or *N*-iodosuccinimide (1−4 equiv) in an organic solvent ($CH_3CN$, DMF, $CH_2Cl_2$) (2 mL/mmol) was stirred at room temperature for 1 h then was filtered through a short pad of Celite. The filtrate was diluted with $CH_2Cl_2$,



DOI: 10.1021/acs.jmedchem.7b01714
J. Med. Chem. 2018, 61, 4348−4369

and the resulting solution was washed with water, dried over $Na_2SO_4$, filtered, and concentrated under reduced pressure to afford the reaction crude product that was either used unpurified or purified as described.

*General Procedure B: Suzuki Coupling Using $Pd(PPh_3)_4$.* To a slurry of the halide derivative, boronic acid (2 equiv), and a base (2 equiv of $K_3PO_4$, $Na_2CO_3$) in a mixture of 1,4-dioxane (10 mL/mmol) and $H_2O$ (2 mL/mmol) was added $Pd(PPh_3)_4$ (0.2 equiv). The reaction mixture was heated at 90 °C for 12 h under argon atmosphere, then cooled and filtered through a short pad of Celite. The filtrate was concentrated to dryness under reduced pressure, and the residue was purified as described in each case.

*General Procedure C: Ester Hydrolysis.* To a solution of carboxylic ester in a mixture of THF (4 mL/mmol) and $CH_3OH$ (1.28 mL/mmol) were added LiOH (8 equiv) and water (1.28 mL/mmol). The reaction mixture was stirred for 5 h at room temperature and then concentrated to a smaller volume, diluted with water (2.56 mL/mmol), and acidified with an aqueous solution of HCl until pH 3. The precipitate was isolated by filtration and dried to afford the desired product.

*General Procedure D: Amide Coupling.* To a solution of carboxylic acid derivative in DMF (2.8 mL/mmol) were added sequentially *N*-methylmorpholine (2 equiv), HATU (1.5 equiv), and the amine (1.5 equiv). The reaction mixture was stirred at room temperature for 3 h under nitrogen atmosphere. The reaction mixture was diluted with water (2 mL/mmol). At this stage, if the product precipitated it was isolated by filtration, or if it stayed in solution the aqueous phase was extracted with an organic solvent. The combined extracts were dried over $Na_2SO_4$, filtered, and concentrated. The residue was purified as described.

**Synthesis.** *N-(3-(4-Hydroxyphenyl)imidazo[1,2-a]pyrazin-6-yl)-acetamide (**4**). Step 1: N-(Imidazo[1,2-a]pyrazin-6-yl)acetamide (**2a**).* To a slurry of 6-bromoimidazo[1,2-*a*]pyrazine (1.00 g, 5.00 mmol), acetamide (380 mg, 6.50 mmol), and $K_2CO_3$ (1.38 g, 10.0 mmol) in toluene (30 mL) were added CuI (47 mg, 0.05 mmol) and *N,N*-dimethylethylenediamine (44 mg, 0.50 mmol). The resulting mixture was heated at 90 °C for 12 h under an inert atmosphere. The reaction mixture was filtered through a short pad of Celite, and the filtrate was concentrated under reduced pressure. The residue was purified by flash column chromatography (silica gel, eluent *n*-hexane/EtOAc 50:50) to afford *N*-(imidazo[1,2-*a*]pyrazin-6-yl)acetamide (500 mg, 56%). $^1$H NMR (400 MHz, DMSO-$d_6$) $\delta$ (ppm): 10.55 (s, 1H), 9.24 (s, 1H), 8.91 (s, 1H), 8.23 (s, 1H), 7.76 (s, 1H), 2.10 (s, 3H); MS (ESI) *m*/*z* 177 $[C_8H_8N_4O+H]^+$.

*Step 2: N-(3-Bromoimidazo[1,2-a]pyrazin-6-yl)acetamide (**3a**).* A solution of *N*-(imidazo[1,2-*a*]pyrazin-6-yl)acetamide (1.00 g, 5.00 mmol) and *N*-bromosuccinimide (900 mg, 5.1 mmol) in $CH_2Cl_2$ (10 mL) was stirred at room temperature for 1 h and then filtered through a short pad of Celite. The filtrate was diluted with $CH_2Cl_2$, and the resulting solution was washed with water, dried over $Na_2SO_4$, filtered, and concentrated under reduced pressure to afford *N*-(3-bromoimidazo[1,2-*a*]pyrazin-6-yl)acetamide (700 mg, 53%). $^1$H NMR (400 MHz, $CDCl_3$) $\delta$ (ppm): 9.15 (s, 1H), 8.83 (s, 1H), 7.90 (bs, 1H), 7.79 (s, 1H), 2.28 (s, 3H); MS (ESI) *m*/*z* 255 $[C_8H_7BrN_4O]^+$.

*Step 3: N-(3-(4-Hydroxyphenyl)imidazo[1,2-a]pyrazin-6-yl)-acetamide (**4**).* To a slurry of *N*-(3-bromoimidazo[1,2-*a*]pyrazin-6-yl)acetamide (600 mg, 2.35 mmol), (4-hydroxyphenyl)boronic acid (290 mg, 2.82 mmol), and $Na_2CO_3$ (620 mg, 5.80 mmol) in a mixture of $H_2O$ (2.00 mL) and DMF (20 mL) were successively added $Pd(OAc)_2$ (26 mg, 0.11 mmol) and a solution of triphenylphosphine (120 mg, 0.47 mmol) in 1,4-dioxane. The reaction mixture was stirred at 90 °C for 12 h under argon and then filtered through a short pad of Celite. The filtrate was concentrated under reduced pressure, and the residue was purified by column chromatography (silica gel, eluent *n*-hexane/EtOAc 25:75) to afford *N*-(3-(4-hydroxyphenyl)imidazo[1,2-*a*]pyrazin-6-yl)acetamide (70 mg, 11%, AUC HPLC 95.1%). $^1$H NMR (400 MHz, DMSO-$d_6$) $\delta$ (ppm): 10.61 (s, 1H), 9.90 (s, 1H), 9.23 (s, 1H), 8.95 (s, 1H), 7.86 (s, 1H), 7.46 (d, *J* = 8.8 Hz, 2H), 6.96 (d, *J* = 8.4 Hz, 2H), 2.08 (s, 3H). $^{13}$C NMR (100 MHz, DMSO-$d_6$) $\delta$ (ppm): 159.07, 154.65, 142.03, 136.38, 127.44, 126.63, 125.10, 114.48, 112.90, 112.44, 55.56, 28.35; MS (ESI) *m*/*z* 269.1 $[C_{14}H_{12}N_4O_2+H]^+$.

*N-(3-(4-Hydroxyphenyl)imidazo[1,2-a]pyrazin-6-yl)benzamide (**5**). Step 1: N-(Imidazo[1,2-a]pyrazin-6-yl)benzamide (**2b**).* To a solution of 6-bromoimidazo[1,2-*a*]pyrazine (500 mg, 2.52 mmol), benzamide (305 mg, 2.51 mmol), and $K_2CO_3$ (500 mg, 1.37 mmol) in toluene (20 mL) were added CuI (23 mg, 0.12 mmol) and *N,N*-dimethylethylenediamine (8 mg, 0.09 mmol). The resulting mixture was heated at 110 °C for 2 h, and the reaction mixture was filtered through a short pad of Celite. The filtrate was concentrated and purified by flash column chromatography (silica gel, eluent *n*-hexane/EtOAc 50:50) to afford *N*-(imidazo[1,2-*a*]pyrazin-6-yl)benzamide (200 mg, 33%) as an off-white solid. $^1$H NMR (400 MHz, $CDCl_3$) $\delta$ (ppm): 9.43 (s, 1H), 8.90 (s, 1H), 8.52 (s, 1H), 7.95 (d, *J* = 7.2 Hz, 2H), 7.82 (d, *J* = 7.2 Hz, 2H), 7.45 (t, *J* = 7.2 Hz, 3H); MS (ESI) *m*/*z* 239 $[C_{13}H_{10}N_4O+H]^+$.

*Step 2: N-(3-Bromoimidazo[1,2-a]pyrazin-6-yl)benzamide (**3b**).* A solution of *N*-(imidazo[1,2-*a*]pyrazin-6-yl)benzamide (200 mg, 0.84 mmol) and *N*-bromosuccinimide (148 mg, 0.83 mmol) in $CHCl_3$ (9.00 mL) was stirred at room temperature for 5 min, and the reaction mixture was filtered through a short pad of Celite. The filtrate was diluted with $CH_2Cl_2$ and washed with water. The organic phase was dried and concentrated under reduced pressure. The residue was purified by flash column chromatography (silica gel, eluent *n*-hexane/EtOAc 80:20) to afford *N*-(3-bromoimidazo[1,2-*a*]pyrazin-6-yl)-benzamide (100 mg, 37%) as a yellow solid. $^1$H NMR (400 MHz, $CDCl_3$) $\delta$ (ppm): 9.38 (s, 1H), 9.86 (s, 1H), 8.59 (s, 1H), 7.97 (d, *J* = 7.2 Hz, 2H), 7.82 (d, *J* = 8.0 Hz, 1H), 7.55 (t, *J* = 2.4 Hz, 3H); MS (ESI) *m*/*z* 317 $[C_{13}H_9BrN_4O+H]^+$.

*Step 3: N-(3-(4-Hydroxyphenyl)imidazo[1,2-a]pyrazin-6-yl)-benzamide (**5**).* To a mixture of *N*-(3-bromoimidazo[1,2-*a*]pyrazin-6-yl)benzamide (100 mg, 0.13 mmol), (4-hydroxyphenyl)boronic acid (52 mg, 0.37 mmol), $Na_2CO_3$ (83 mg, 0.78 mmol), and $H_2O$ (1.0 mL) in DMF (5.0 mL) were added $Pd(OAc)_2$ (3 mg, 0.01 mmol) and triphenylphosphine (16 mg, 0.06 mmol) in 1,4-dioxane. The reaction mixture was heated at 90 °C for 2 h under argon and filtered through a short pad of Celite. The filtrate was concentrated under reduced pressure, and the residue was purified by flash column chromatography (silica gel, eluent *n*-hexane/EtOAc 25:75) to afford *N*-(3-(4-hydroxyphenyl)imidazo[1,2-*a*]pyrazin-6-yl)benzamide (5 mg, 5%, AUC HPLC 98.4%) as an off white solid. $^1$H NMR (400 MHz, DMSO-$d_6$) $\delta$ (ppm): 10.98 (s, 1H), 9.42 (s, 1H), 9.04 (s, 1H), 8.02 (d, *J* = 7.2 Hz, 2H), 7.91 (s, 1H), 7.61−7.48 (m, 5H), 6.99 (d, *J* = 8.4 Hz, 2H); MS (ESI) *m*/*z* 331 $[C_{19}H_{14}N_4O_2+H]^+$.

*4-(6-Bromoimidazo[1,2-a]pyrazin-3-yl)phenol (**7a**).* The title compound was prepared in a similar fashion as described in general procedure B starting from 3-bromo-6-iodoimidazo[1,2-*a*]pyrazine (15 g, 4.63 mmol) and 4-hydroxyphenylboronic acid (6.4 g, 4.64 mmol). The residue was purified by column chromatography (silica gel, eluent *n*-hexane/EtOAc 50:50) to afford 4-(6-bromoimidazo[1,2-*a*]pyrazin-3-yl)phenol (10.0 g, 77%) as yellow solid. $^1$H NMR (400 MHz, DMSO-$d_6$) $\delta$ (ppm): 9.92 (s, 1H), 8.98 (s, 1H), 8.62 (s, 1H), 7.98 (s, 1H), 7.52 (d, *J* = 8.4 Hz, 2H), 6.93 (d, *J* = 8.4 Hz, 2H); MS (ESI), *m*/*z* 290 $[C_{12}H_8BrN_3O]^+$.

*4-(6-Phenylimidazo[1,2-a]pyrazin-3-yl)phenol (**8**).* A mixture of 4-(6-bromoimidazo[1,2-*a*]pyrazin-3-yl)phenol (93 mg, 0.32 mmol), $Cs_2CO_3$ (203 mg, 0.64 mmol), phenylboronic acid (59 mg, 0.48 mmol), and $PdCl_2$(dppf) (47 mg, 0.064 mmol) in a mixture of DMF (2.5 mL) and $H_2O$ (0.5 mL) was heated in microwave reactor at 140 °C for 30 min. The reaction mixture was concentrated to dryness under reduced pressure. The residue was purified by flash column chromatography (silica gel, DCM/methanol 10:1) to afford 4-(6-phenylimidazo[1,2-*a*]pyrazin-3-yl)phenol (61 mg, 66%, AUC HPLC 99.6%) as a yellow solid; mp: 249.7−251.3 °C; $^1$H NMR (400 MHz, MeOD-$d_4$) $\delta$ (ppm): 9.08 (d, *J* = 1.2 Hz, 1H), 8.65 (d, *J* = 1.2 Hz, 1H), 7.92 (d, *J* = 7.3 Hz, 2H), 7.83 (s, 1H), 7.54 (d, *J* = 8.6 Hz, 2H), 7.46 (t, *J* = 7.4 Hz, 2H), 7.43−7.36 (m 1H), 7.02 (d, *J* = 8.6 Hz, 2H), 4.56 (s, 1H); $^{13}$C NMR (100 MHz, MeOD-$d_4$) $\delta$ (ppm): 160.01, 143.47, 141.59, 141.35, 137.80, 134.78, 130.99, 129.99, 129.90, 129.87,


DOI: 10.1021/acs.jmedchem.7b01714
J. Med. Chem. 2018, 61, 4348−4369

127.64, 119.58, 117.53, 114.37; MS (ESI) $m/z$ 288.20 $[C_{18}H_{13}N_3O+H]^+$.

*(4-(3-Bromoimidazo[1,2-a]pyrazin-6-yl)phenyl)(4-methylpiperazin-1-yl)methanone (**15**). Step 1: Ethyl 4-(Imidazo[1,2-a]pyrazin-6-yl)benzoate (**9**).* To a solution of 6-bromoimidazo[1,2-*a*]pyrazine (30 g, 151 mmol) in toluene (400 mL) were sequentially added $Cs_2CO_3$ (123 g, 378 mmol), 4-(ethoxycarbonyl)phenylboronic acid (35.2 g, 181 mmol), and $PdCl_2$(dppf) (3.70 g, 4.50 mmol). The reaction mixture was stirred at 90 °C for 12 h under argon then, was filtered through Celite. The filtrate was concentrated under reduced pressure, and the residue was purified by flash column chromatography (silica gel, eluent *n*-hexane/EtOAc 70:30) to afford ethyl 4-(imidazo[1,2-*a*]pyrazin-6-yl)benzoate (16 g, 39%) as yellow solid. $^1$H NMR (400 MHz, DMSO-$d_6$) $\delta$ (ppm): 9.35 (s, 1H), 9.17 (s, 1H), 8.15 (d, $J$ = 8.4 Hz, 2H), 8.03 (d, $J$ = 8.4 Hz, 2H), 7.88 (s, 1H), 7.79 (s, 1H), 4.32 (q, $J$ = 6.8 Hz, 2H), 1.44 (t, $J$ = 7.2 Hz, 3H); MS (ESI) $m/z$ 268 $[C_{15}H_{13}N_3O_2+H]^+$.

*Step 2: Ethyl 4-(3-Bromoimidazo[1,2-a]pyrazin-6-yl)benzoate (**10**).* To a solution of ethyl 4-(imidazo[1,2-*a*]pyrazin-6-yl)benzoate (16.0 g, 59.8 mmol) in a mixture of $CCl_4$ (200 mL) and $CH_3OH$ (50 mL) was added *N*-bromosuccinamide (12.7 g, 71.8 mmol). The reaction mixture was stirred at room temperature for 30 min, then filtered through Celite. The filtrate was concentrated under reduced pressure, and the residue was suspended in water and extracted with $CH_2Cl_2$. The organic phase was concentrated under reduced pressure to afford ethyl 4-(3-bromoimidazo[1,2-*a*]pyrazin-6-yl)benzoate (18.0 g, 87%) as a yellow solid. $^1$H NMR (400 MHz, DMSO-$d_6$) $\delta$ (ppm): 9.17 (s, 1H), 8.78 (s, 1H), 8.28 (d, $J$ = 8.4 Hz, 2H), 8.09 (d, $J$ = 8.0 Hz, 2H), 7.94 (s, 1H), 4.34 (q, $J$ = 7.2 Hz, 2H), 1.35 (t, $J$ = 7.2 Hz, 3H); MS (ESI) $m/z$ 345 $[C_{15}H_{12}BrN_3O_2]^+$

*Step 3: 4-(3-Bromoimidazo[1,2-a]pyrazin-6-yl)benzoic Acid (**12**).* To a solution of ethyl 4-(3-bromoimidazo[1,2-*a*]pyrazin-6-yl)benzoate (27.0 g, 77.9 mmol) in a mixture of THF (300 mL) and $CH_3OH$ (100 mL) were added LiOH (26.0 g, 623 mmol) and water (100 mL). The reaction mixture was stirred for 5 h at room temperature and then concentrated under reduced pressure. The residue was diluted with water (200 mL) and was acidified with an aqueous solution of HCl until pH 3. The precipitate was isolated by filtration and dried to afford 4-(3-bromoimidazo[1,2-*a*]pyrazin-6-yl)benzoic acid (14.0 g, 56%) as a white solid. $^1$H NMR (400 MHz, $CDCl_3$) $\delta$ (ppm): 9.17 (s, 1H), 8.68 (s, 1H), 8.25 (d, $J$ = 8.4 Hz 2H), 8.09 (d, $J$ = 8.0 Hz, 2H), 7.99 (s, 1H); MS (ESI) $m/z$ 316 $[C_{13}H_8BrN_3O_2]^+$.

*Step 4: (4-(3-Bromoimidazo[1,2-a]pyrazin-6-yl)phenyl)(4-methylpiperazin-1-yl)methanone (**15**).* *N*-Methylmorpholine (4.8 mL, 44.0 mmol), HATU (12.5 g, 33 mmol) and *N*-methylpiperazine (3.6 mL, 33 mmol) were added to a solution of 4-(3-bromoimidazo[1,2-*a*]pyrazin-6-yl)benzoic acid (7.0 g, 22 mmol) in DMF (70 mL). The resulting reaction mixture was stirred at room temperature for 10 h. The reaction mixture was diluted with water, and the precipitate was isolated by filtration to afford (4-(3-bromoimidazo[1,2-*a*]pyrazin-6-yl)phenyl)(4-methylpiperazin-1-yl)methanone (6.0 g, 68%) as a yellow solid. $^1$H NMR (400 MHz, $CDCl_3$) $\delta$ (ppm): 9.15 (d, $J$ = 1.2 Hz, 1H), 8.44−8.43 (d, $J$ = 1.2 Hz, 1H), 8.05 (d, $J$ = 8.0 Hz, 2H), 7.83 (s, 1H), 7.57 (d, $J$ = 8.0 Hz, 2H), 3.85 (bs, 2H), 3.51 (bs, 2H), 2.53 (bs, 2H), 2.41 (bs, 2H), 2.35 (s, 3H); MS (ESI) $m/z$ 400 $[C_{18}H_{18}BrN_5O]^+$.

*(4-(3-Iodoimidazo[1,2-a]pyrazin-6-yl)phenyl)(4-methylpiperazin-1-yl)methanone (**16**). Step 1: Ethyl 4-(3-Iodoimidazo[1,2-a]pyrazin-6-yl)benzoate (**11**).* To a solution of ethyl 4-(imidazo[1,2-*a*]pyrazin-6-yl)benzoate (8.00 g, 29.9 mmol) in DMF (200 mL) was added *N*-iodosuccinimide (8.10 g, 36.0 mmol), and the mixture was heated at 60 °C for 2 h and then poured into ice water. The precipitate was isolated by filtration and dried to afford ethyl 4-(3-iodoimidazo[1,2-*a*]pyrazin-6-yl)benzoate (11 g, 94%) as a yellow solid. $^1$H NMR (400 MHz, DMSO-$d_6$) $\delta$ (ppm): 9.13 (s, 1H), 8.80 (s, 1H), 8.29 (d, $J$ = 8.4 Hz, 2H), 8.07 (d, $J$ = 8.4 Hz, 2H), 8.00 (s, 1H), 4.37−4.31 (m, 2H), 1.34 (t, $J$ = 7.2 Hz, 3H); MS (ESI) $m/z$ 393 $[C_{15}H_{12}IN_3O_2]^+$.

*Step 2: 4-(3-Iodoimidazo[1,2-a]pyrazin-6-yl)benzoic Acid (**13**).* A solution of ethyl 4-(3-iodoimidazo[1,2-*a*]pyrazin-6-yl)benzoate (11 g, 30.5 mmol) and LiOH·$H_2O$ (5.00 g, 121 mmol) in THF/$CH_3OH$/$H_2O$ (200/50/50 mL) was stirred at room temperature for 12 h. The reaction mixture was concentrated under reduced pressure to a smaller volume. The residue was diluted with water (20 mL) and acidified with an aqueous solution of HCl until pH 2. The precipitate was isolated by filtration and dried to afford 4-(3-iodoimidazo[1,2-*a*]pyrazin-6-yl)benzoic acid (8.00 g, 72%) as an off-white solid. $^1$H NMR (400 MHz, DMSO-$d_6$) $\delta$ (ppm): 9.12 (s, 1H), 8.78 (s, 1H), 8.26 (d, $J$ = 8.4 Hz, 2H), 8.06 (d, $J$ = 8.4 Hz, 2H), 8.05 (s, 1H); MS (ESI) $m/z$ 366 $[C_{13}H_8IN_3O_2+H]^+$.

*Step 3: (4-(3-Iodoimidazo[1,2-a]pyrazin-6-yl)phenyl)(4-methylpiperazin-1-yl)methanone (**16**).* *N*-Methylmorpholine (12 mL, 109.1 mmol), HATU (26.6 g, 77.84 mmol), and *N*-methylpiperazine (8.6 mL, 77.5 mmol) were added sequentially to a solution of 4-(3-iodoimidazo[1,2-*a*]pyrazin-6-yl)benzoic acid (19.0 g, 52.03 mmol) in DMF (170 mL). The resulting mixture was stirred under nitrogen at room temperature for 3 h and diluted with water (200 mL). The precipitate was isolated by filtration and was dried to afford (4(4-(3-iodoimidazo[1,2-*a*]pyrazin-6-yl)phenyl)(4-methylpiperazin-1-yl)-methanone (16.0 g, 70%) as an off-white solid. $^1$H NMR (400 MHz, $CDCl_3$) $\delta$ (ppm): 9.15 (d, $J$ = 1.2 Hz, 1H), 8.44 (d, $J$ = 1.2 Hz, 1H), 8.05 (d, $J$ = 8.0 Hz, 2H), 7.83 (s, 1H), 7.57 (d, $J$ = 8.0 Hz, 2H), 3.85 (bs, 2H), 3.51 (bs, 2H), 2.53 (bs, 2H), 2.41 (bs, 2H), 2.35 (s, 3H). $^{13}$C NMR (100 MHz, DMSO-$d_6$) $\delta$ (ppm): 169.14, 162.81, 142.88, 142.85, 142.75, 138.95, 137.45, 136.47, 127.99, 126.81, 116.56, 70.28, 54.98, 46.01, 36.26, 31.25; MS (ESI) $m/z$ 447 $[C_{18}H_{18}IN_5O]^+$.

*4-(3-(4-Hydroxyphenyl)imidazo[1,2-a]pyrazin-6-yl)benzamide (**19**). Step 1: 4-(3-Bromoimidazo[1,2-a]pyrazin-6-yl)benzamide (**14**).* The title compound was prepared in a similar fashion as described in general procedure D starting from 4-(3-bromoimidazo[1,2-*a*]pyrazin-6-yl)benzoic acid (0.5 g, 1.57 mmol) and a 7 N solution of ammonia in THF (0.7 mL, 4.9 mmol). The residue was purified by flash column chromatography (silica gel, eluent $CH_2Cl_2$/$CH_3OH$ 90:10) to afford 4-(3-bromoimidazo[1,2-*a*]pyrazin-6-yl)benzamide (0.2 g, 40%). $^1$H NMR (400 MHz, DMSO-$d_6$) $\delta$ (ppm): 9.16 (s, 1H), 8.80 (s, 1H), 8.08 (d, $J$ = 8.0 Hz, 2H), 7.88 (s, 1H), 7.56 (d, $J$ = 8.4 Hz, 2H); MS (ESI) $m/z$ 317 $[C_{13}H_9BrN_4O]^+$.

*Step 2: 4-(3-(4-Hydroxyphenyl)imidazo[1,2-a]pyrazin-6-yl)-benzamide (**19**).* The title compound was prepared in a similar fashion as described in general procedure B with 4-(3-bromoimidazo-[1,2-*a*]pyrazin-6-yl)benzamide (0.5 g, 1.58 mmol) and 4-hydroxyphenylboronic acid (0.44, 3.16 mmol) as starting materials. The reaction crude product was purified by flash column chromatography (silica gel, eluent $CH_2Cl_2$/$CH_3OH$ 85:15) and by preparative HPLC to afford 4-(3-(4-hydroxyphenyl)imidazo[1,2-*a*]pyrazin-6-yl)benzamide (100 mg, 19%, AUC HPLC 98%) as an off-white solid. $^1$H NMR (400 MHz, DMSO-$d_6$) $\delta$ (ppm): 9.20 (s, 1H), 8.85 (s, 1H), 8.12 (d, $J$ = 8.0 Hz, 2H), 7.97 (d, $J$ = 8.4 Hz, 2H), 7.92 (s, 1H), 7.56 (d, $J$ = 8.4 Hz, 2H), 7.40 (bs, 1H), 6.91 (d, $J$ = 8.4 Hz, 2H). $^{13}$C NMR (100 MHz, DMSO-$d_6$) $\delta$ (ppm): 166.90, 159.05, 142.21, 139.15, 138.45, 136.99, 133.74, 133.31, 128.86, 127.38, 127.35, 125.34, 116.15, 115.98, 113.30; MS (ESI) $m/z$ 331 $[C_{19}H_{14}N_4O_2+H]^+$.

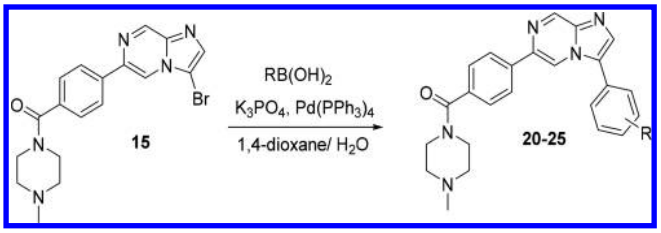


*Compounds **20**−**24**.* These compounds were prepared in a fashion similar to that described in general procedure B to afford the desired product after purification by flash column chromatography through silica gel. The details are summarized in Table 8, and their characterization data follow.

*(4-(3-(4-Hydroxyphenyl)imidazo[1,2-a]pyrazin-6-yl)phenyl)(4-methylpiperazin-1-yl)methanone (**20**).* $^1$H NMR (400 MHz, $CDCl_3$) $\delta$ (ppm): 9.21 (s, 1H), 8.54 (s, 1H), 7.96 (d, $J$ = 8.4 Hz, 2H), 7.83 (s, 1H), 7.54 (d, $J$ = 8.4 Hz, 2H), 7.43 (d, $J$ = 8.4 Hz, 2H), 7.06 (d, $J$ = 8.8


DOI: 10.1021/acs.jmedchem.7b01714
J. Med. Chem. 2018, 61, 4348−4369

**Table 8. Purification Eluent, Yield, and Purity for Compounds 20−24**

| compd | R | purification eluent | amount (yield, purity) |
|---|---|---|---|
| **20** | 4-OH | $CH_2Cl_2/CH_3OH$ 95:5 | 30 mg (19%, >99%) |
| **21** | H | *n*-hexane/EtOAc 60:40 | 60 mg (25%, >99%) |
| **22** | 2-OH | $CH_2Cl_2/CH_3OH$ 98:2 | 15 mg (15%, 96.8%) |
| **23** | 3-OH | $CH_2Cl_2/CH_3OH$ 95:5 | 60 mg (9%, 98.5%) |
| **24** | 4-$CH_3$ | *n*-hexane/EtOAc 30:70 | 50 mg (50%, >99% |

Hz, 2H), 3.86 (bs, 2H), 3.51 (bs, 2H), 2.53 (bs, 2H), 2.41 (bs, 2H), 2.35 (s, 3H). $^{13}$C NMR (100 MHz, DMSO-$d_6$) $\delta$ (ppm): 168.07, 157.49, 142.24, 139.20, 137.14, 136.86, 135.10, 133.86, 128.95, 127.04, 126.83, 125.62, 117.39, 115.63, 113.09, 53.86, 46.44, 44.90, 40.70, 37.41; MS (ESI) *m*/*z* 414 $[C_{24}H_{23}N_5O_2+H]^+$.

*(4-Methylpiperazin-1-yl)(4-(3-phenylimidazo[1,2-a]pyrazin-6-yl)-phenyl)methanone (**21**).* Mp: 222.9−223.9 °C, $^1$H NMR (400 MHz, $CDCl_3$) $\delta$ (ppm): 9.25 (s, *J* = 1.2 Hz, 1H), 8.44 (s, 1H), 8.06 (d, *J* = 8.0 Hz, 2H), 7.83 (s, 1H), 7.58−7.56 (m, 4H), 7.50 (d, 3H) 3.85 (bs, 4H), 3.51 (bs, 4H), 2.41 (bs, 3H). $^{13}$C NMR (100 MHz, DMSO-$d_6$) $\delta$ (ppm): 169.14, 143.46, 140.70, 138.47, 137.84, 136.26, 135.80, 129.92, 129.21, 128.35, 128.05, 127.90, 127.78, 126.75, 116.11, 114.40, 54.85, 47.58, 46.01, 41.92; MS (ESI) *m*/*z* 398 $[C_{24}H_{23}N_5O+H]^+$.

*(4-(3-(2-Hydroxyphenyl)imidazo[1,2-a]pyrazin-6-yl)phenyl)(4-methylpiperazin-1-yl)methanone (**22**).* $^1$H NMR (400 MHz, DMSO-$d_6$) $\delta$ (ppm) 9.24 (s, 1H), 9.09 (s, 1H), 8.85 (s, 1H), 8.14 (d, *J* = 8.8 Hz, 2H), 7.99 (s, 1H), 7.62−7.56 (q, *J* = 8.4 Hz, 4H), 6.99 (d, 2H), 3.84 (bs, 4H), 3.15 (s, 4H), 2.31 (s, 3H). $^{13}$C NMR (100 MHz, DMSO-$d_6$) $\delta$ (ppm): 169.14, 155.58, 142.83, 140.41, 138.01, 137.27, 136.14, 136.06, 131.86, 131.15, 128.01, 126.45, 126.31, 120.15, 116.87, 116.55, 114.914, 54.78, 47.55, 47.93, 45.93, 41.92. ; MS (ESI) *m*/*z* 414 $[C_{24}H_{23}N_5O_2+H]^+$.

*(4-(3-(3-Hydroxyphenyl)imidazo[1,2-a]pyrazin-6-yl)phenyl)(4-methylpiperazin-1-yl)methanone (**23**).* $^1$H NMR (400 MHz, $CD_3OD$) $\delta$ (ppm): 9.15 (s, 1H), 8.74 (s, 1H), 8.06 (d, *J* = 8.0 Hz, 2H), 7.83 (s, 1H), 7.58−7.56 (m, 3H), 7.50 (d, 3H) 3.85 (bs, 4H), 3.51 (bs, 4H), 2.31 (s, 3H); MS (ESI) *m*/*z* 414 $[C_{24}H_{23}N_5O_2+H]^+$.

*(4-Methylpiperazin-1-yl)(4-(3-p-tolylimidazo[1,2-a]pyrazin-6-yl)-phenyl)methanone (**24**).* $^1$H NMR (400 MHz, DMSO-$d_6$) $\delta$ (ppm): 9.25 (s, 1H), 8.10 (s, 1H), 7.93−7.91 (d, *J* = 8.4 Hz, 2H), 7.83 (s, 1H), 7.51−7.47 (m, 4H), 7.41−7.40 (d, *J* = 8.8 Hz, 2H), 7.25 (s, 1H), 3.85 (bs, 1H), 3.50 (s, 4H), 2.55 (bs, 2H), 2.32 (s, 3H), 2.25 (s, 3H). $^{13}$C NMR (100 MHz, DMSO-$d_6$) $\delta$ (ppm): 169.13, 143.41, 140.58, 138.81, 138.36, 137.86, 136.24, 135.48, 130.46, 128.31, 127.90, 127.83, 126.71, 125.12, 114.32, 54.84, 47.54, 46.03, 41.95, 21.40; MS (ESI) *m*/*z* 411.5 $[C_{25}H_{25}N_5O+H]^+$

*4-(6-(4-(4-Methylpiperazine-1-carbonyl)phenyl)imidazo[1,2-a]-pyrazin-3-yl)benzoic Acid (**25**). Step 1: Ethyl 4-(6-(4-(4-Methylpiperazine-1-carbonyl)phenyl)imidazo[1,2-a]pyrazin-3-yl)benzoate.* The title compound was prepared in a similar fashion as described in general procedure B starting from (4-(3-bromoimidazo[1,2-*a*]pyrazin-6-yl)phenyl)(4-methylpiperazin-1-yl)methanone (1.00 g, 2.5 mmol) and 4-(ethoxycarbonyl)phenylboronic acid (970 mg, 5.0 mmol). The reaction crude product was purified by flash column chromatography (silica gel, eluent $CHCl_3$/MeOH 94:6) to afford ethyl 4-(6-(4-(4-methylpiperazine-1-carbonyl)phenyl)imidazo[1,2-*a*]pyrazin-3-yl)-benzoate (600 mg, 55%) as an off-white solid. $^1$H NMR (400 MHz, $CD_3OD$) $\delta$ (ppm) 9.28−9.27 (d, *J* = 1.2 Hz, 1H), 8.64−8.64 (d, *J* = 1.2 Hz, 1H), 8.29−8.27 (d, *J* = 8.0 Hz, 2H), 7.99−7.98 (d, *J* = 2.0 Hz, 2H), 7.96 (s, 1H), 7.74−7.72 (d, *J* = 8.4 Hz, 2H), 7.55−7.53 (d, *J* = 8.4 Hz, 2H), 4.48−4.43 (q, *J* = 7.2 Hz, 2H), 3.84 (bs, 2H), 3.50 (bs, 2H), 2.53 (bs, 2H), 2.39 (bs, 2H), 2.35 (s, 3H), 1.47−1.44 (t, *J* = 7.2 Hz, 3H); MS (ESI) *m*/*z* 470 $[C_{27}H_{27}N_5O_3+H]^+$.

*Step 2: 4-(6-(4-(4-Methylpiperazine-1-carbonyl)phenyl)imidazo-[1,2-a]pyrazin-3-yl)benzoic Acid (**25**).* The title compound was prepared in a similar fashion as described in general procedure C starting from ethyl 4-(6-(4-(4-methylpiperazine-1-carbonyl)phenyl)-imidazo[1,2-*a*]pyrazin-3-yl)benzoate (600 mg, 1.28 mmol) to afford the 4-(6-(4-(4-methylpiperazine-1-carbonyl)phenyl)imidazo[1,2-*a*]-pyrazin-3-yl)benzoic acid as a solid (450 mg, 80%, AUC HPLC 97.1%). $^1$H NMR (400 MHz, DMSO-$d_6$) $\delta$ (ppm): 9.28 (s, 1H), 9.01 (s, 1H), 8.17−8.11 (m, 5H), 7.94−7.92 (d, *J* = 8.0 Hz, 2H), 7.50−7.48 (d, *J* = 8.0 Hz, 2H), 3.61 (bs, 4H), 2.32 (bs, 4H), 2.19 (s, 3H). $^{13}$C NMR (100 MHz, DMSO-$d_6$) $\delta$ (ppm): 169.23, 167.36, 143.57, 141.09, 138.71, 137.93, 136.65, 135.91, 132.26, 130.95, 130.75, 128.21, 127.97, 126.97, 126.89, 114.83, 53.746, 42.02, 12.67; MS (ESI) *m*/*z* 440 $[C_{25}H_{23}N_5O_3+H]^+$.

*N-Hydroxy-4-(6-(4-(4-methylpiperazine-1-carbonyl)phenyl)-imidazo[1,2-a]pyrazin-3-yl)benzamide (**26**). Step 1: 4-(6-(4-(4-Methylpiperazine-1-carbonyl)phenyl)imidazo[1,2-a]pyrazin-3-yl)-N-((tetrahydro-2H-pyran-2-yl)oxy)benzamide.* To a solution of 4-(6-(4-(4-methylpiperazine-1-carbonyl)phenyl)imidazo[1,2-*a*]pyrazin-3-yl)benzoic acid (50 mg, 0.113 mmol) in a mixture of $CH_2Cl_2$ (3 mL) and DMF (1 mL) was added sequentially DIPEA (83 $\mu$L, 0.48 mmol), HOBt (32 mg, 0.24 mmol), EDCI·HCl (45 mg, 0.24 mmol), and *O*-(tetrahydro-2*H*-pyran-2-yl)hydroxylamine (26 mg, 0.23 mmol). The reaction mixture was stirred at room temperature under inert atmosphere for 12 h, diluted with $H_2O$ (3 mL), and extracted with $CH_2Cl_2$ (3 × 10 mL). The combined organic layer was dried over $Na_2SO_4$, filtered, and concentrated under reduced pressure. The crude residue was purified by flash column chromatography to afford 4-(6-(4-(4-methylpiperazine-1-carbonyl)phenyl)imidazo[1,2-*a*]pyrazin-3-yl)-*N*-((tetrahydro-2*H*-pyran-2-yl)oxy)benzamide (44.6 mg, 73%, AUC HPLC 94.5%) as a white solid. $^1$H NMR (600 MHz, DMSO-$d_6$) $\delta$ (ppm): 11.81 (bs, 1H), 9.30 (s, 1H), 9.00 (s, 1H), 8.19 (s, 1H), 8.16 (d, *J* = 12 Hz, 2H), 7.99 (dd, *J* = 10.6, 8.3 Hz, 4H), 7.51 (d, *J* = 12 Hz, 2H), 5.08−5.04 (m, 1H), 4.13−4.06 (m, 1H), 3.70−3.53 (m, 3H), 3.45−3.25 (m, 2H), 2.43−2.27 (m, 4H), 2.22 (s, 3H), 1.79−1.73 (m, 3H), 1.63−1.53 (m, 3H); $^{13}$C NMR (125 MHz, DMSO-$d_6$) $\delta$ (ppm): 169.1, 164.0, 143.5, 141.0, 138.6, 137.7, 136.3, 132.4, 131.1, 128.7, 128.1, 127.8, 127.0, 126.8, 114.6, 101.5, 61.8, 54.9, 46.0, 28.3, 25.1, 18.7; MS (ESI) *m*/*z* 541 $[C_{30}H_{32}N_6O_4+H]^+$.

*Step 2: N-Hydroxy-4-(6-(4-(4-methylpiperazine-1-carbonyl)-phenyl)imidazo[1,2-a]pyrazin-3-yl)benzamide (**26**).* To a solution of 4-(6-(4-(4-methylpiperazine-1-carbonyl)phenyl)imidazo[1,2-*a*]-pyrazin-3-yl)-*N*-((tetrahydro-2*H*-pyran-2-yl)oxy)benzamide (10 mg, 0.018 mmol) in a mixture of $CH_3CN$/MeOH (1:1, 0.6 mL) was added a 1 M aqueous solution of HCl (110 $\mu$L, 0.11 mmol) at room temperature. The reaction mixture was stirred for 4 h and was concentrated *in vacuo*. The residue was diluted with hexane, dried over $Na_2SO_4$, filtered, and concentrated to dryness under reduced pressure to yield the *N*-hydroxy-4-(6-(4-(4-methylpiperazine-1-carbonyl)-phenyl)imidazo[1,2-*a*]pyrazin-3-yl)benzamide as a hydrochloride salt (5.3 mg, 63%, AUC HPLC > 99%), light yellow solid. $^1$H NMR (600 MHz, DMSO-$d_6$) $\delta$ (ppm): 11.39 (bs, 1H), 9.35 (s, 1H), 9.04 (s, 1H), 8.26 (s, 1H), 8.20 (d, *J* = 8.4 Hz, 2H), 8.00 (d, *J* = 7.8 Hz, 2H), 7.95 (d, *J* = 8.4 Hz, 2H), 7.59 (d, *J* = 8.4 Hz, 2H), 4.39−3.60 (m, 6H), 3.05−3.15 (m, 2H), 2.77 (s, 3H); $^{13}$C NMR (125 MHz, DMSO-$d_6$) $\delta$ (ppm): 168.8, 163.3, 142.5, 139.6, 138.4, 137.5, 134.7, 134.5, 132.6, 129.7, 127.8, 127.7, 127.6, 126.7, 126.4, 114.4, 51.8, 41.9; MS (ESI) *m*/*z* 457 $[C_{25}H_{24}N_6O_3+H]^+$.

*4-(6-(4-(4-Methylpiperazine-1-carbonyl)phenyl)imidazo[1,2-a]-pyrazin-3-yl)benzonitrile (**27**).* The title compound was prepared in a similar fashion as described in general procedure B starting from (4-(3-bromoimidazo[1,2-*a*]pyrazin-6-yl)phenyl)(4-methylpiperazin-1-yl)-methanone (200 mg, 0.50 mmol) and 4-cyanophenylboronic acid (110 mg, 0.75 mmol). The reaction crude product was purified by flash column chromatography (silica gel, eluent $CH_2Cl_2$/MeOH 95:5 to 90:10) to afford 4-(6-(4-(4-methylpiperazine-1-carbonyl)phenyl)-imidazo[1,2-*a*]pyrazin-3-yl)benzonitrile (154.7 mg, 73%, AUC HPLC > 99%) as a yellow solid, mp: 223.9−225.1 °C. $^1$H NMR (300 MHz, DMSO-$d_6$) $\delta$ (ppm): 9.31 (s, 1H), 9.04 (s, 1H), 8.25 (s, 1H), 8.16 (d, *J* = 8.1 Hz, 2H), 8.11−8.04 (m, 4H), 7.51 (d, *J* = 8.1 Hz, 2H), 3.63 (bs, 2H), 3.46−3.20 (m, 2H), 2.32 (bs, 4H), 2.20 (s, 3H). $^{13}$C NMR (100 MHz, DMSO-$d_6$) $\delta$ (ppm): 168.04, 142.47, 140.18, 137.77, 136.63, 136.07, 135.32, 132.61, 131.74, 127.76, 126.79, 125.80, 125.21, 118.08, 113.92, 110.09, 53.743, 46.44, 44.93, 40.87; MS (ESI) *m*/*z* 423 $[C_{25}H_{22}N_6O+H]^+$.

*(4-(3-(4-Chlorophenyl)imidazo[1,2-a]pyrazin-6-yl)phenyl)(4-methylpiperazin-1-yl)methanone (**28**).* The title compound was



DOI: 10.1021/acs.jmedchem.7b01714
J. Med. Chem. 2018, 61, 4348−4369

prepared in a similar fashion as described in general procedure B starting from (4-(3-iodoimidazo[1,2-*a*]pyrazin-6-yl)phenyl)(4-methylpiperazin-1-yl)methanone (150 mg, 0.34 mmol) and 4-chlorophenylboronic acid (79 mg, 0.50 mmol). The reaction crude product was purified by flash column chromatography (silica gel, eluent $CH_2Cl_2$/MeOH 95:5 to 90:10) to afford (4-(3-(4-chlorophenyl)imidazo[1,2-*a*]pyrazin-6-yl)phenyl)(4-methylpiperazin-1-yl)methanone (128.4 mg, 66%, AUC HPLC > 99%) as a yellow solid, mp: 208.0−208.5 °C. $^1$H NMR (400 MHz, $CDCl_3$) $\delta$ (ppm): 9.24 (d, $J$ = 1.4 Hz, 1H), 8.54 (d, $J$ = 1.4 Hz, 1H), 7.95 (d, $J$ = 8.4 Hz, 2H), 7.89 (s, 1H), 7.60−7.55 (m, 4H), 7.52 (d, $J$ = 8.4 Hz, 2H), 3.82 (bs, 2H), 3.49 (s, 2H), 2.50−2.33 (m, 7H); $^{13}$C NMR (100 MHz, $CDCl_3$) $\delta$ (ppm) 169.78, 143.84, 140.70, 139.63, 137.76, 136.14, 135.34, 135.33, 129.98, 129.36, 127.84, 126.45, 126.41, 126.24, 112.54, 55.27, 54.79, 46.03; MS (ESI) $m/z$ 432 $[C_{24}H_{22}ClN_5O+H]^+$.

*(4-methylpiperazin-1-yl)(4-(3-(4-(trifluoromethyl)phenyl)-imidazo[1,2-a]pyrazin-6-yl)phenyl)methanone (**29**).* The title compound was prepared in a similar fashion as described in general procedure B starting from (4-(3-iodoimidazo[1,2-*a*]pyrazin-6-yl)-phenyl)(4-methylpiperazin-1-yl)methanone (200 mg, 0.45 mmol) and 4-(trifluoromethyl)phenylboronic acid (101 mg, 0.54 mmol). The reaction crude product was purified by column chromatography (silica gel, eluent $CH_2Cl_2$/MeOH 95:5 to 90:10) to afford (4-methylpiperazin-1-yl)(4-(3-(4-(trifluoromethyl)phenyl)imidazo[1,2-*a*]pyrazin-6-yl)phenyl)methanone (150 mg, 72%, AUC HPLC 97%) as a yellow solid, mp: 190.5−191.5 °C. $^1$H NMR (400 MHz, MeOD-$d_4$) $\delta$ (ppm): 9.18 (s, 1H), 8.91 (s, 1H), 8.11 (d, $J$ = 8.20 Hz, 2H), 8.08 (s, 1H), 8.00 (d, $J$ = 8.2 Hz, 2H), 7.94 (d, $J$ = 8.2 Hz, 2H), 7.54 (d, $J$ = 8.3 Hz, 2H), 3.81 (bs, 2H), 3.54 (bs, 2H), 2.55−2.47 (m, 4H), 2.36 (s, 3H); $^{13}$C NMR (100 MHz, MeOD-$d_4$) $\delta$ (ppm) 172.00, 143.96, 142.16, 140.93, 139.31, 136.90, 136.43, 132.89 (q, $J$ = 1.3 Hz), 131.85 (q, $J$ = 32.4 Hz), 129.77, 128.75, 128.19, 127.90, 127.57, 125.52 (q, $J$ = 269.6 Hz), 115.24, 45.99; MS (ESI) $m/z$ 466 $[C_{25}H_{22}F_3N_5O+H]^+$.

*(4-(3-(4-(Difluoromethyl)phenyl)imidazo[1,2-a]pyrazin-6-yl)-phenyl)(4-methylpiperazin-1-yl)methanone (**30**).* The title compound was prepared in a similar fashion as described in general procedure B starting from (4-(3-bromoimidazo[1,2-*a*]pyrazin-6-yl)-phenyl)(4-methylpiperazin-1-yl)methanone (200 mg, 0.5 mmol) and 2-(4-(difluoromethyl)phenyl)-4,4,5,5-tetramethyl-1,3,2-dioxaborolane (317 mg, 1.25 mmol). The reaction crude product was purified by flash column chromatography (silica gel, eluent $CHCl_3$/MeOH 96.5:3.5%) and by preparative HPLC to give (4-(3-(4-(difluoromethyl)phenyl)imidazo[1,2-*a*]pyrazin-6-yl)phenyl)(4-methylpiperazin-1-yl)methanone (50 mg, 23%, AUC HPLC > 99%) as an off-white solid; mp: 73−86 °C. $^1$H NMR (400 MHz, $CDCl_3$) $\delta$ (ppm): 9.26 (s, 1 H), 8.60 (s, 1H), 7.96−7.94 (m, 3H), 7.77−7.71 (m, 4H), 7.52 (d, $J$ = 8.0 Hz, 2H), 6.76 (t, $J$ = 5.6 Hz, 1H), 3.82 (bs, 2H), 3.47 (bs, 2H), 2.51 (bs, 2H), 2.34 (bs, 2H), 2.33 (s, 3H). $^{13}$C NMR (100 MHz, DMSO-$d_6$) $\delta$ (ppm): 169.13, 143.50, 140.93, 138.64, 137.75, 136.37, 136.31, 134.40 (t, $J$ = 22.33, $CF_2H$), 130.62, 128.66, 127.86, 127.28, 127.22, 127.16, 126.92, 126.81, 117.55, 115.20, 114.65, 112.86, 55.00, 47.59, 46.03, 41.93; MS (ESI) $m/z$ 448.46 $[C_{25}H_{23}F_2N_5O+H]^+$.

*4-(6-(4-(4-Methylpiperazine-1-carbonyl)phenyl)imidazo[1,2-a]-pyrazin-3-yl)benzamide (**31**).* The title compound was prepared in a similar fashion as described in general procedure B starting from (4-(3-iodoimidazo[1,2-*a*]pyrazin-6-yl)phenyl)(4-methylpiperazin-1-yl)-methanone and 4-carbamoylphenylboronic acid (110.6 mg, 0.671 mmol). The reaction crude product was purified by flash column chromatography (silica gel, eluent $CH_2Cl_2$/MeOH 90:10) to afford 4-(6-(4-(4-methylpiperazine-1-carbonyl)phenyl)imidazo[1,2-*a*]pyrazin-3-yl)benzamide (189 mg, 96%, AUC HPLC 96%) as a light brown solid. $^1$H NMR (400 MHz, DMSO-$d_6$) $\delta$ (ppm): 9.29 (d, $J$ = 1.2 Hz, 1H), 9.01 (d, $J$ = 1.2 Hz, 1H), 8.18−8.09 (m, 6H), 7.95 (d, $J$ = 8.4 Hz, 2H), 7.52−7.50 (m, 3H), 3.63−3.31 (m, 4H), 2.35 (bs, 4H), 2.22 (s, 3H); MS (ESI) $m/z$ 441 $[C_{25}H_{24}N_6O_2+H]^+$.

*(4-(3-(4-Hydroxyphenyl)imidazo[1,2-a]pyrazin-6-yl)phenyl)-(morpholino)methanone (**32**). Step 1: (4-(3-Bromoimidazo[1,2-a]pyrazin-6-yl)phenyl)(morpholino)methanone (**17**).* To a solution of 4-(3-bromoimidazo[1,2-*a*]pyrazin-6-yl)benzoic acid (8.00 g, 25.14 mmol) in DMF (70 mL), were sequentially added *N*-methylmorpholine (5.5 mL, 50.28 mmol), HATU (14.4 g, 37.71 mmol), and morpholine (3.32 mL, 37.71 mmol). The reaction mixture was stirred at room temperature for 3 h under nitrogen, then diluted with water (50 mL). The precipitate was isolated by filtration and dried to afford (4-(3-bromoimidazo[1,2-*a*]pyrazin-6-yl)phenyl)(morpholino)-methanone (6.40 g, 66%) as an off-white solid. $^1$H NMR (400 MHz, $CDCl_3$) $\delta$ (ppm): 9.15 (d, $J$ = 1.2 Hz, 1H), 8.44 (d, $J$ = 1.2 Hz, 1H), 8.05 (d, $J$ = 8.0 Hz, 2H), 7.83 (s, 1H), 7.57 (d, $J$ = 8.0 Hz, 2H), 3.85 (bs, 2H), 3.51 (bs, 2H), 2.53 (bs, 2H), 2.41 (bs, 2H); MS (ESI) $m/z$ 387 $[C_{17}H_{15}BrN_4O_2+H]^+$.

*Step 2: (4-(3-(4-Hydroxyphenyl)imidazo[1,2-a]pyrazin-6-yl)-phenyl)(morpholino)methanone (**32**).* The title compound was prepared in a similar fashion as described in general procedure B starting from (4-(3-bromoimidazo[1,2-*a*]pyrazin-6-yl)phenyl)-(morpholino)methanone and 4-hydroxyphenylboronic acid. The reaction crude product was purified by flash column chromatography (silica gel, eluent $CH_2Cl_2$/$CH_3OH$ 95:5) to afford (4-(3-(4-hydroxyphenyl)imidazo[1,2-*a*]pyrazin-6-yl)phenyl)(morpholino)-methanone (150 mg, 32%, AUC HPLC 97.6%) as an off-white solid. $^1$H NMR (400 MHz, $CD_3OD$) $\delta$ (ppm): 9.88 (s, 1H), 9.21 (s, 1H), 8.83 (s, 1H), 8.11 (d, $J$ = 8.0 Hz, 2H), 7.94 (s, 1H), 7.61 (d, $J$ = 8.4 Hz, 2H), 7.51 (d, $J$ = 8.4 Hz, 2H), 6.97 (d, $J$ = 8.4 Hz, 2H), 3.60 (bs, 8H). $^{13}$C NMR (100 MHz, DMSO-$d_6$) $\delta$ (ppm): 168.20, 157.48, 142.25, 139.21, 137.12, 136.97, 134.74, 133.87, 128.95, 127.04, 126.97, 126.87, 125.62, 117.40, 115.63, 113.12, 65.49, 47.14, 41.49; MS (ESI) $m/z$ 401 $[C_{23}H_{20}N_4O_3+H]^+$.

*4-(6-(4-(Morpholine-4-carbonyl)phenyl)imidazo[1,2-a]pyrazin-3-yl)benzonitrile (**33**). Step 1: (4-(3-Iodoimidazo[1,2-a]pyrazin-6-yl)phenyl)(morpholino)methanone (**18**).* *N*-Methylmorpholine (3.0 mL, 7.5 mmol), HATU (7.5 g, 27 mmol), and morpholine (1.26 g, 14.85 mmol) were added sequentially to a solution of 4-(3-iodoimidazo[1,2-*a*]pyrazin-6-yl)benzoic acid (5.0 g, 3.25 mmol) in DMF (10 mL), and the resulting mixture was stirred at room temperature for 3 h under nitrogen. The reaction mixture was diluted with water (50 mL), and the precipitate was isolated by filtration and dried to afford (4-(3-iodoimidazo[1,2-*a*]pyrazin-6-yl)phenyl)-(morpholino)methanone (2.0 g, 65%) as an off-white solid. $^1$H NMR (400 MHz, $CDCl_3$) $\delta$ (ppm): 9.10 (s, 1H), 8.50 (s, 1H), 8.10 (d, 2H), 7.90 (s, 1H), 7.60 (d, 2H), 3.4−3.9 (m, 8H). $^{13}$C NMR (100 MHz, DMSO-$d_6$) $\delta$ (ppm): 169.23, 142.84, 142.74, 138.90, 137.54, 136.09, 130.28, 128.12, 126.78, 116.57, 70.31, 66.57, 48.13, 42.55; MS (ESI) $m/z$ 434 $[C_{17}H_{15}IN_4O_2+H]^+$.

*Step 2: 4-(6-(4-(Morpholine-4-carbonyl)phenyl)imidazo[1,2-a]-pyrazin-3-yl)benzonitrile (**33**).* The title compound was prepared in a similar fashion as described in general procedure B starting from (4-(3-iodoimidazo[1,2-*a*]pyrazin-6-yl)phenyl)(morpholino)methanone (200 mg, 0.52 mmol) and 4-cyanophenylboronic acid. The reaction crude product was purified by flash column chromatography (silica gel, eluent DCM/MeOH 95:5) to afford 4-(6-(4-(morpholine-4-carbonyl)phenyl)imidazo[1,2-*a*]pyrazin-3-yl)benzonitrile (100 mg, 53%, AUC HPLC 95%) as a yellow solid; mp: 238.2−239.5 °C. $^1$H NMR (400 MHz, $CD_3OD$) $\delta$ (ppm): 9.17 (d, $J$ = 0.7 Hz, 1H), 8.55 (d, $J$ = 1.0 Hz, 1H), 7.95−7.86 (m, 3H), 7.80 (d, $J$ = 8.3 Hz, 2H), 7.72 (d, $J$ = 8.3 Hz, 2H), 7.43 (d, $J$ = 8.2 Hz, 2H), 3.88−3.22 (m, 8H). $^{13}$C NMR (100 MHz, DMSO-$d_6$) $\delta$ (ppm): 169.24, 143.55, 141.25, 138.81, 137.80, 137.15, 136.02, 133.68, 132.81, 128.82, 128.01, 126.86, 126.28, 119.16, 115.01, 111.16, 66.554, 48.15, 42.53; MS (ESI) $m/z$ 410 $[C_{24}H_{19}N_5O_2+H]^+$.

*1-(4-(4-(3-(4-Hydroxyphenyl)imidazo[1,2-a]pyrazin-6-yl)-benzoyl)piperazin-1-yl)ethanone (**36**). Step 1: Ethyl 4-(3-(4-Hydroxyphenyl)imidazo[1,2-a]pyrazin-6-yl)benzoate (**34a**).* The title compound was prepared in a similar fashion as described in general procedure B starting from 4-(6-bromoimidazo[1,2-*a*]pyrazin-3-yl)phenol (3.00 g, 10.3 mmol) and 4-(ethoxycarbonyl)-phenylboronic acid (2.20 g, 11.3 mmol). The residue was purified by flash column chromatography (silica gel, eluent $CH_2Cl_2$/$CH_3OH$ 97:3) to afford ethyl 4-(3-(4-hydroxyphenyl)imidazo[1,2-*a*]pyrazin-6-yl)benzoate (600 mg, 16%) as a yellow solid. $^1$H NMR (400 MHz,


DOI: 10.1021/acs.jmedchem.7b01714
J. Med. Chem. 2018, 61, 4348−4369

DMSO-$d_6$) $\delta$ (ppm): 9.87 (s, 1H), 9.22 (s, 1H), 8.89 (s, 1H), 7.95 (s, 1H), 7.80 (s, 1H), 7.73 (s, 1H), 7.61 (d, $J$ = 8.0 Hz, 4H), 6.98 (d, $J$ = 8.0 Hz, 2H), 4.34 (q, $J$ = 7.2 Hz, 2H), 1.35 (t, $J$ = 7.2 Hz, 3H); MS (ESI), $m/z$ 360.3 $[C_{21}H_{17}N_3O_3+H]^+$.

*Step 2: 4-(3-(4-Hydroxyphenyl)imidazo[1,2-a]pyrazin-6-yl)-benzoic Acid (**35a**).* The title compound was prepared in a similar fashion as described in general procedure C starting from ethyl 4-(3-(4-hydroxyphenyl)imidazo[1,2-*a*]pyrazin-6-yl)benzoate (600 mg, 1.60 mmol) to afford 4-(3-(4-hydroxyphenyl)imidazo[1,2-*a*]pyrazin-6-yl)-benzoic acid (100 mg, 20%) as a light yellow solid. $^1$H NMR (400 MHz, DMSO-$d_6$) $\delta$ (ppm): 9.91 (s, 1H), 9.23 (s, 1H), 8.89 (s, 1H), 7.97 (s, 1H), 7.78 (s, 1H), 7.73 (d, $J$ = 8.0 Hz, 2H), 7.61 (d, $J$ = 8.0 Hz, 2H), 6.98 (d, $J$ = 8.0 Hz, 2H); MS (ESI), $m/z$ 332.3 $[C_{19}H_{13}N_3O_3+H]^+$.

*Step 3: 1-(4-(4-(3-(4-Hydroxyphenyl)imidazo[1,2-a]pyrazin-6-yl)-benzoyl)piperazin-1-yl)ethanone (**36**).* The title compound was prepared in a similar fashion as described in general procedure D starting from 4-(3-(4-hydroxyphenyl)imidazo[1,2-*a*]pyrazin-6-yl)-benzoic acid (200 mg, 0.60 mmol) and 1-(piperazin-1-yl)ethanone (92 mg, 0.71 mmol). The precipitate was isolated by filtration and dried to afford 1-(4-(4-(3-(4-hydroxyphenyl)imidazo[1,2-*a*]pyrazin-6-yl)benzoyl)piperazin-1-yl)ethanone (103 mg, 38%, AUC HPLC 95.5%) as a yellow solid; mp: 199.9−200.7 °C; $^1$H NMR (400 MHz, $CDCl_3$) $\delta$ (ppm): 9.90 (s, 1H), 9.20 (s, 1H), 8.85 (s, 1H), 8.13 (d, $J$ = 8.0 Hz, 2H), 7.90 (s, 1H), 7.60 (d, $J$ = 8.0 Hz, 2H), 7.52 (d, $J$ = 8.0 Hz, 2H), 6.98 (d, $J$ = 6.0 Hz, 2H), 3.40−3.70 (m, 8H), 2.10 (s, 3H). $^{13}$C NMR (100 MHz, DMSO-$d_6$) $\delta$ (ppm): 168.36, 167.89, 157.49, 142.25, 139.22, 137.10, 137.02, 134.85, 133.88, 128.95, 127.05, 126.96, 125.63, 117.39, 115.63, 113.14, 44.87, 41.29, 40.11, 20.64; MS (ESI) $m/z$ 442 $[C_{25}H_{23}N_5O_3+H]^+$.

*4-(6-(4-(4-(Dimethylamino)piperidine-1-carbonyl)phenyl)-imidazo[1,2-a]pyrazin-3-yl)benzonitrile (**37**). Step 1: 4-(6-Bromoimidazo[1,2-a]pyrazin-3-yl)benzonitrile (**7b**).* To a solution of 3-bromo-6-iodoimidazo[1,2-*a*]pyrazine (6.0 g, 18.6 mmol), 4-cyanophenylboronic acid (3.67 g, 27.9 mmol), in 1,4-dioxane (100 mL), were successively added an aqueous solution of $Na_2CO_3$ (4.0 g, 37.2 mmol) and $Pd(PPh_3)_4$ (1.42 g, 13 mmol). The reaction mixture was heated at 90 °C for 3 h then, filtered through a short pad of Celite. The filtrate was concentrated under reduced pressure, and the residue was purified by flash column chromatography (silica gel, eluent *n*-hexane/EtOAc 50:50) to afford 4-(6-bromoimidazo[1,2-*a*]pyrazin-3-yl)benzonitrile (3.6 g, 67%) as a yellow solid which was used in next step without further purification. $^1$H NMR (400 MHz, DMSO-$d_6$) $\delta$ (ppm): 9.10 (s, 1H), 8.89 (s, 1H), 8.38 (s, 1H), 8.10−7.92 (m, 4H); MS (ESI), $m/z$ 299.13 $[C_{13}H_7BrN_4]^+$.

*Step 2: Ethyl 4-(3-(4-Cyanophenyl)imidazo[1,2-a]pyrazin-6-yl)-benzoate (**34b**).* A mixture of 4-(6-bromoimidazo[1,2-*a*]pyrazin-3-yl)benzonitrile (5.00 g, 16.7 mmol), 4-(ethoxycarbonyl)phenylboronic acid (4.90 g, 25.2 mmol), $Na_2CO_3$ (4.40 g, 41.5 mmol), and $Pd(PPh_3)_4$ (386 mg, 0.33 mmol) in $H_2O$ (5.00 mL) and DMF (100 mL) was heated at 90 °C for 2 h. The reaction mixture was diluted with water. The precipitate was isolated by filtration and dried under vacuum to afford ethyl 4-(3-(4-cyanophenyl)imidazo[1,2-*a*]pyrazin-6-yl)benzoate (2.80 g, 46%) as an off-white solid. $^1$H NMR (400 MHz, DMSO-$d_6$) $\delta$ (ppm): 9.28 (s, 1H), 9.07 (s, 1H), 8.25 (s, 1H), 8.22 (d, $J$ = 6.0 Hz, 2H), 8.08−8.02 (m, 6H), 4.38−4.33 (m, 2H), 1.36 (t, $J$ = 7.2 Hz, 3H); MS (ESI) $m/z$ 369 $[C_{22}H_{16}N_4O_2+H]^+$.

*Step 3: 4-(3-(4-Cyanophenyl)imidazo[1,2-a]pyrazin-6-yl)benzoic Acid (**35b**).* A mixture of ethyl 4-(3-(4-cyanophenyl)imidazo[1,2-*a*]pyrazin-6-yl)benzoate (2.80 g, 7.61 mmol) and LiOH·$H_2O$ (1.25 g, 30.5 mmol) in THF/$CH_3OH$/$H_2O$ (50 mL/20 mL/20 mL) was stirred at room temperature for 12 h. The reaction mixture was concentrated under reduced pressure. The residue was diluted with water (20 mL) and an aqueous solution of HCl until pH 2. The precipitate was isolated by filtration and dried to afford 4-(3-(4-cyanophenyl)imidazo[1,2-*a*]pyrazin-6-yl)benzoic acid (2.00 g, 80%) as an off-white solid. $^1$H NMR (400 MHz, DMSO-$d_6$) $\delta$ (ppm): 9.30 (s, 1H), 9.08 (s, 1H), 8.22 (d, $J$ = 9.6 Hz, 3H), 8.06−8.02 (m, 6H); MS (ESI) $m/z$ 341 $[C_{20}H_{12}N_4O_2+H]^+$.

*Step 4: 4-(6-(4-(4-(Dimethylamino)piperidine-1-carbonyl)-phenyl)imidazo[1,2-a]pyrazin-3-yl)benzonitrile (**37**).* The title compound was prepared in a similar fashion as described in general procedure B starting from 4-(3-(4-cyanophenyl)imidazo[1,2-*a*]-pyrazin-6-yl)benzoic acid (180 mg, 0.52 mmol) and *N*,*N*-dimethyl-4-aminopiperidine (1.5 equiv). The reaction crude product was purified by flash column chromatography (silica gel, eluent $CH_2Cl_2$/$CH_3OH$ 96:4) to afford 4-(6-(4-(4-(dimethylamino)piperidine-1-carbonyl)-phenyl)imidazo[1,2-*a*]pyrazin-3-yl)benzonitrile (65 mg, 22%, AUC HPLC 96%) as an off-white solid, mp: 177.2−178.5 °C; $^1$H NMR (400 MHz, DMSO) $\delta$(ppm): 9.31 (d, $J$ = 1.1 Hz, 1H), 9.04 (d, $J$ = 1.1 Hz, 1H), 8.24 (s, 1H), 8.15 (d, $J$ = 8.2 Hz, 2H), 8.10−8.00 (m, 4H), 7.50 (d, $J$ = 8.2 Hz, 2H), 4.46 (bs, 1H), 3.65 (bs, 1H), 3.20−2.75 (m, 2H), 2.45−2.30 (m, 1H), 2.33 (s, 6H), 1.95−1.60 (m, 2H), 1.50−1.30 (m, 2H); MS (ESI) $m/z$ 451.20 $[C_{27}H_{26}N_6O+H]^+$.

*4-(6-(4-(4-Methylpiperazine-1-carbonyl)phenyl)imidazo[1,2-b]-pyridazin-3-yl)benzonitrile (**39**).* The title compound was prepared in a similar fashion as described in general procedure B starting from 4-(6-chloroimidazo[1,2-*b*]pyridazin-3-yl)benzonitrile (200 mg, 0.785 mmol) and (4-(4-methylpiperazine-1-carbonyl)phenyl)boronic acid HCl salt (268 mg, 0.942 mmol). The residue was purified by flash column chromatography (silica gel, eluent $CH_2Cl_2$/MeOH 95:5 to 90:10) to afford 4-(6-(4-(4-methylpiperazine-1-carbonyl)phenyl)-imidazo[1,2-*b*]pyridazin-3-yl)benzonitrile (91.2 mg, 43%, AUC HPLC 99%) as a yellow solid. $^1$H NMR (400 MHz, $CDCl_3$) $\delta$ (ppm): 8.30 (d, $J$ = 8.6 Hz, 2H), 8.23−8.21 (m, 2H), 8.06 (d, $J$ = 8.4 Hz, 2H), 7.81 (d, $J$ = 8.6 Hz, 2H), 7.66−7.61 (m, 3H), 7.31 (bs, 1H), 3.97−3.74 (m, 4H), 2.84 (bs, 4H), 2.56 (s, 3H); $^{13}$C NMR (100 MHz, $CDCl_3$) $\delta$ (ppm): 169.57, 165.35, 151.41, 140.15, 137.01, 136.67, 134.25, 132.82, 132.60, 128.12, 127.49, 127.05, 126.70, 126.54, 118.75, 116.71, 111.15, 53.78, 44.43; MS (ESI) $m/z$ 423 $[C_{25}H_{22}N_6O+H]^+$.

*4-(6-(4-(Morpholine-4-carbonyl)phenyl)imidazo[1,2-b]pyridazin-3-yl)benzonitrile (**40**).* To a solution of 4-(6-chloroimidazo[1,2-*b*]pyridazin-3-yl)benzonitrile (150 mg, 0.59 mmol) in DMF (2.5 mL) and water (0.5 mL) under inert atmosphere were added $Cs_2CO_3$ (384 mg, 1.18 mmol), morpholino(4-(4,4,5,5-tetramethyl-1,3,2-dioxaborolan-2-yl)phenyl)methanone (279 mg, 0.88 mmol), and $PdCl_2$(dppf) (86 mg, 0.118 mmol). The resulting mixture was heated in a microwave reactor at 140 °C for 30 min and then diluted with $H_2O$ (10 mL) and extracted with DCM (3 × 15 mL). The combined organic layer was dried over $Na_2SO_4$, filtered, and concentrated under reduced pressure. The crude residue was purified by flash column chromatography (silica gel, eluent $CH_2Cl_2$/MeOH 95:5 to 90:10) to afford 4-(6-(4-(morpholine-4-carbonyl)phenyl)imidazo[1,2-*b*]-pyridazin-3-yl)benzonitrile (72.1 mg, 35%, AUC HPLC 96%) as a yellow solid; mp: 263−266 °C; IR (neat) $\nu$ cm$^{-1}$: 3096.85 (C−H), 2213.41 (C≡N), 1627.03 (C═O). $^1$H NMR (400 MHz, $CDCl_3$) $\delta$ (ppm): 8.31−8.25 (m, 4H), 8.06−8.05 (m, 2H), 7.82−7.81 (m, 2H), 7.70−7.61 (m, 3H), 3.78−3.53 (m, 8H); $^{13}$C NMR (100 MHz, $CDCl_3$) $\delta$ (ppm): 169.39, 151.86, 137.43, 136.45, 133.24, 132.63, 132.52, 128.14, 128.08, 127.47, 127.26, 126.86, 126.30, 118.66, 117.32, 111.39, 66.87, 48.21, 42.67; MS (ESI) $m/z$ 410 $[C_{24}H_{19}N_5O_2+H]^+$. Anal. Calculated for $C_{24}H_{19}N_5O_2$•0.75($H_2O$): C, 68.15; H, 4.89; N, 16.56. Found: C, 68.05; H, 4.63; N, 16.41.

*4-(6-(4-(Piperazine-1-carbonyl)phenyl)imidazo[1,2-b]pyridazin-3-yl)benzonitrile (**42**). Step 1: 4-(3-(4-Cyanophenyl)imidazo[1,2-b]pyridazin-6-yl)benzoic Acid (**41**).* To a solution of 4-(6-chloroimidazo[1,2-*b*]pyridazin-3-yl)benzonitrile (484 mg, 1.9 mmol) in DMF (20 mL) and water (4 mL) under an inert atmosphere were added $Cs_2CO_3$ (1.24 g, 3.8 mmol), 4-boronobenzoic acid (473 mg, 2.85 mmol), and $Pd(dppf)_2Cl_2$ (278 mg, 0.38 mmol). The resulting mixture was heated at 90 °C for 18 h and then diluted with water (20 mL) and extracted with DCM (3 × 40 mL). The combined organic layer was dried over $Na_2SO_4$, filtered, and concentrated under reduced pressure. The residue was purified by flash column chromatography (silica gel, eluent $CH_2Cl_2$/MeOH 95:5 to 90:10) to afford 4-(3-(4-cyanophenyl)imidazo[1,2-*b*]pyridazin-6-yl)benzoic acid (310 mg, 48%) as a brown solid, mp: 260.1−261.3 °C. $^1$H NMR (400 MHz, DMSO-$d_6$) $\delta$ (ppm): 8.54 (s, 1H), 8.51 (d, $J$ = 8.6 Hz, 2H), 8.40 (d, $J$ = 9.6 Hz, 1H), 8.26 (d, $J$ = 8.4 Hz, 2H), 8.13 (d, $J$ = 8.4 Hz, 2H), 8.03



DOI: 10.1021/acs.jmedchem.7b01714
J. Med. Chem. 2018, 61, 4348−4369

(d, $J$ = 8.6 Hz, 2H), 8.02 (d, $J$ = 9.6 Hz, 1H); $^{13}$C NMR (100 MHz, DMSO-$d_6$) $\delta$ (ppm): 167.53, 151.29, 140.69, 138.86, 136.06, 133.37, 133.25, 130.47, 127.70, 127.19, 126.81, 126.48, 119.37, 117.53, 110.05. MS (ESI) $m/z$ 341 $[C_{20}H_{12}N_4O_2+H]^+$.

*Step 2: 4-(6-(4-(Piperazine-1-carbonyl)phenyl)imidazo[1,2-b]-pyridazin-3-yl)benzonitrile (**42**).* The title compound was prepared in a similar fashion as described in general procedure D starting from 4-(3-(4-cyanophenyl)imidazo[1,2-*b*]pyridazin-6-yl)benzoic acid (764 mg, 1.57 mmol) and *tert*-butyl piperazine-1-carboxylate (347 mg, 2.36 mmol) to afford the reaction crude product. MS (ESI) $m/z$ 509 $[C_{29}H_{28}N_6O+H]^+$. The crude product was carried forth to the next step without further purification.

To a solution of *tert*-butyl 4-(4-(3-(4-cyanophenyl)imidazo[1,2-*b*]pyridazin-6-yl)benzoyl)piperazine-1-carboxylate (~1.57 mmol) in DCM (1 mL) was added TFA (1 mL). The resulting mixture was stirred at room temperature for 18 h and concentrated under reduced pressure. The residue was purified by flash column chromatography to afford 4-(6-(4-(piperazine-1-carbonyl)phenyl)imidazo[1,2-*b*]-pyridazin-3-yl)benzonitrile (200 mg, 31% over 2 steps, AUC HPLC 98%) as a yellow solid. $^1$H NMR (400 MHz, MeOD-$d_4$) $\delta$ (ppm): 8.45 (d, $J$ = 8.6 Hz, 2H), 8.34 (s, 1H), 8.26−8.22 (m, 3H), 7.95 (d, $J$ = 9.6 Hz, 1H), 7.89 (d, $J$ = 8.6 Hz, 2H), 7.71 (d, $J$ = 8.4 Hz, 2H), 3.87 (bs, 4H), 3.27 (bs, 4H); $^{13}$C NMR (100 MHz, MeOD-$d_4$) $\delta$ (ppm): 171.80, 152.88, 138.46, 137.54, 135.28, 134.19, 133.64, 129.23, 129.11, 128.72, 128.27, 127.85, 127.14, 119.70, 118.58, 112.00, 44.56; MS (ESI) $m/z$ 409 $[C_{24}H_{20}N_6O+H]^+$.

*4-(6-(4-(4-(Dimethylamino)piperidine-1-carbonyl)phenyl)-imidazo[1,2-b]pyridazin-3-yl)benzonitrile (**45**). Step 1: (4-(3-Bromoimidazo[1,2-b]pyridazin-6-yl)phenyl)(4-(dimethylamino)-piperidin-1-yl)methanone (**44**).* To a solution of 4-(3-bromoimidazo-[1,2-*b*]pyridazin-6-yl)benzoic acid (500 mg, 1.57 mmol) in DMF (5 mL) was added NMM (317 mg, 3.14 mmol) followed by HATU (754.7 mg, 2.35 mmol), and the solution was stirred for 30 min at room temperature prior to the addition of *N,N*-dimethylpiperidin-4-amine (221 mg, 1.72 mmol). The mixture was stirred for an additional 16 h. The reaction mixture was diluted with EtOAc and washed with water and brine. The organic layer was dried over anhydrous $Na_2SO_4$, filtered, and concentrated under reduced pressure. The crude residue was purified by flash column chromatography (silica gel, eluent $CH_2Cl_2$/MeOH 95:5) to afford (4-(3-bromoimidazo[1,2-*b*]pyridazin-6-yl)phenyl)(4-(dimethylamino)piperidin-1-yl)methanone (350 mg, 52%) as an off-white solid. MS (ESI) $m/z$ 429 $[C_{20}H_{22}BrN_5O+H]^+$.

*Step 2: 4-(6-(4-(4-(Dimethylamino)piperidine-1-carbonyl)-phenyl)imidazo[1,2-b]pyridazin-3-yl)benzonitrile (**45**).* To a mixture of (4-(3-bromoimidazo[1,2-*b*]pyridazin-6-yl)phenyl)(4-(dimethylamino)piperidin-1-yl)methanone (350 mg, 0.817 mmol), 4-cyanophenylboronic acid (144 mg, 0.981 mmol), and $K_3PO_4$ (346 mg, 1.63 mmol) in 1,4-dioxane (25 mL) and water (5 mL) was added $Pd(PPh_3)_4$ (47 mg, 0.04 mmol). The reaction mixture was heated at 90 °C for 6 h under an argon atmosphere, then diluted with water (200 mL). The precipitate was isolated by filtration, then purified by flash column chromatography (silica gel, eluent $CHCl_3$/MeOH 95:5) to afford 4-(6-(4-(4-(dimethylamino)piperidine-1-carbonyl)phenyl)-imidazo[1,2-*b*]pyridazin-3-yl)benzonitrile (150 mg, 41%, AUC HPLC 98.9%) as a yellow solid; mp: 123−127 °C; $^1$H NMR (400 MHz, $CDCl_3$) $\delta$ (ppm): 8.78 (d, $J$ = 8.7 Hz, 1H), 8.52 (s, 1H), 8.30 (d, $J$ = 8.2 Hz, 2H), 8.23 (d, $J$ = 8.2 Hz, 2H), 7.76 (d, $J$ = 7.7 Hz, 2H), 7.62 (d, $J$ = 7.6 Hz, 2H), 7.41 (d, $J$ = 7.4 Hz, 1H), 4.9 (bs, 1H), 3.9 (bs, 1H), 3.17 (bs, 1H), 2.91 (bs, 1H), 2.45 (bs, 1H), 2.38 (bs, 6H), 2.08 (bs, 1H), 1.95 (bs, 1H), 1.52 (bs, 2H). $^{13}$C NMR (100 MHz, DMSO-$d_6$) $\delta$ (ppm): 168.63, 151.47, 140.68, 138.52, 136.21, 135.96, 133.42, 133.24, 128.01, 127.74, 127.19, 126.84, 126.47, 119.37, 117.49, 110.06, 61.71, 46.77, 41.76, 28.80, 28.19; MS (ESI) $m/z$ 451.2 $[C_{27}H_{26}N_6O+H]^+$.

*4-(6-(4-(4-Methylpiperazine-1-carbonyl)phenyl)imidazo[1,2-a]-pyridin-3-yl)benzonitrile (**47**).* To a solution of 4-(6-bromoimidazo-[1,2-*a*]pyridin-3-yl)benzonitrile (210 mg, 0.9 mmol), (4-methylpiperazin-1-yl)(4-(4,4,5,5-tetramethyl-1,3,2-dioxaborolan-2-yl)phenyl)-methanone (388 mg, 1.17 mmol), and $NaHCO_3$ (228 mg, 2.71 mmol) in a mixture of DMF (11 mL) and water (2 mL) was added (A-Phos)$_2$PdCl$_2$ (31 mg, 0.04 mmol). The reaction mixture was heated at 90 °C for 1 h under argon, diluted with water, and extracted with EtOAc (3×). The organic phase was washed in turn with water and brine, dried over anhydrous $Na_2SO_4$, filtered, and concentrated under reduced pressure. The residue was purified by preparative TLC to afford of 4-(6-(4-(4-methylpiperazine-1-carbonyl)phenyl)imidazo[1,2-*a*]pyridin-3-yl)benzonitrile (130 mg, 45%, AUC HPLC 98.4%) as a yellow solid; mp: 98−103 °C. $^1$H NMR (400 MHz, $CDCl_3$) $\delta$ (ppm): 8.50 (s, 1H), 7.85−7.79 (m, 4H), 7.74 (d, $J$ = 8.0 Hz, 2H), 7.60−7.52 (m, 5H), 3.83 (bs, 2H), 3.50 (bs, 2H), 2.51 (bs, 2H), 2.37 (bs, 2H), 2.34 (s, 3H). $^{13}$C NMR (75 MHz, $CDCl_3$) $\delta$ (ppm): 169.5, 146.3, 138.5, 135.6, 134.8, 133.8, 133.2, 128.1, 127.8, 127.2, 127.1, 125.6, 124.5, 120.6, 118.7, 118.4, 111.5, 55.3, 47.7, 46.0; MS (ESI) $m/z$ 422.30 $[C_{26}H_{23}N_5O+H]^+$.

*4-(6-(4-(Morpholine-4-carbonyl)phenyl)imidazo[1,2-a]pyridin-3-yl)benzonitrile (**48**).* The title compound was prepared in a similar fashion as described in general procedure B starting from 4-(6-bromoimidazo[1,2-*a*]pyridin-3-yl)benzonitrile (2.0 g, 6.70 mmol) and morpholino(4-(4,4,5,5-tetramethyl-1,3,2-dioxaborolan-2-yl)phenyl)-methanone (2.13 g, 6.71 mmol). The reaction crude product was purified by flash column chromatography (silica gel, eluent $CH_2Cl_2$/MeOH 95:5) to afford 4-(6-(4-(morpholine-4-carbonyl)phenyl)-imidazo[1,2-*a*]pyridin-3-yl)benzonitrile (2.4 g, 88%, AUC HPLC 96.3%) as a yellow solid; mp: 117−120 °C. IR (neat) $\nu$ cm$^{-1}$: 3065.12 (C−H), 2219.20 (C ≡ N), 1623.17(C = O); $^1$H NMR (400 MHz, DMSO-$d_6$) $\delta$ (ppm): 8.80 (s, 1H), 8.01−7.99 (m, 5H), 7.84−7.81 (m, 3H), 7.73 (d, $J$ = 8.8 Hz, 1H), 7.53 (d, $J$ = 8.4 Hz, 2H), 3.72 (bs, 8H); $^{13}$C NMR (150 MHz, DMSO-$d_6$) $\delta$ (ppm): 168.72, 145.74, 137.84, 135.08, 134.92, 133.48, 133.17, 127,82, 127.70, 127.04, 125.74, 125.53, 124.42, 121.82, 118.82, 117.77, 109.79, 66.08; MS (ESI) $m/z$ 409.19 $[C_{25}H_{20}N_4O_2+H]^+$. Anal. Calcd for $C_{25}H_{20}N_4O_2\bullet H_2O$: C, 70.41; H, 5.20; N, 13.14. Found: C, 70.74; H, 5.15; N, 13.15.

**Biology.** MNK1 and MNK2 protein expression, purification, and activation, MNK1 and MNK2 enzymatic assays, eIF4E phosphorylation inhibition in HeLa cell-based Assay, and cell growth inhibition using K562 cell line ($GI_{50}$) were described by Cherian et al.[52]

Kinase selectivity profiling using DiscoveRx proprietary binding assay was described by Karaman et al.[31]

Thermodynamic solubility determination assay was described by Duraiswamy et al.[73]

Cyp inhibition, microsomal metabolic stability, plasma protein binding, Caco-2 permeability, and LogD determination assays are described in Supporting Information.

*In Vivo Studies.* All procedures used for animals studies including *in vivo* anti-tumor efficacy studies and *in vivo* pharmacokinetics studies were approved by the BRC-IACUC Committee (Approval No. 110622) in Singapore. Female Balb/C nude mice of approximately 8−10 weeks old were purchased from Biolasco, Taiwan. CD-1 female mice were purchased from InVivos, Singapore. Food and water were given ad libitum. General protocol for *in vivo* pharmacokinetic studies were described by Ho et al.[74]

*In Vivo PK Studies for **48**. Compound Preparation.* Compound **48** was weighed and dissolved in 1/10 volumes of 100% DMA solution and 1/10 volumes of 100% CremophorEL. The mixtures were vortexed and sonicated in the ultrasonic bath for 30 min. The sterile Milli-Q water (8/10 volumes) was subsequently added and mixed. The final concentration of DMA and CremophorEL in the compound dosing solution was 10% (v/v) each. The final concentration was 0.25 mg/mL for intravenous administration at 1 mg/kg. Compound **48** was dissolved in a mixture of 0.5% methylcellulose and 0.1% Tween80 to a final concentration of 0.625 mg/mL for oral administration at 5 mg/kg.

CD-1 female mice (6−8 weeks old) were weighed, and those selected for dosing were 24 ± 2 g. Three mice were randomly grouped per time point. Mice were administered a single dose of 1 mg/kg of **48** via tail vein injection or a single dose of 5 mg/kg of **48** via oral gavage. The volume of injection for intravenous (i.v.) and oral (p.o.) administration was 4 mL/kg and 8 mL/kg, respectively. Mice were sacrificed using $CO_2$ gas at the predefined time points (predose and post dose at 5 or 10 and 30 min, 1, 2, 4, 8, 16, and 24 h). Blood


DOI: 10.1021/acs.jmedchem.7b01714
J. Med. Chem. 2018, 61, 4348−4369

samples were taken from euthanized mice by cardiac puncture and placed into tubes containing $K_3$EDTA. Plasma was obtained by centrifugation of the blood samples at 15700*g*, 4 °C, for 2 min, and it was stored at −80 °C until analysis. Standard curves of compound were prepared in blank mouse plasma matrices at the concentration ranging from 1 to 1000 ng/mL. First, 10 μL of the internal standard, carbamazepine (50 ng/mL in the mixture of 50% acetonitrile and 0.1% formic acid), and 250 μL of the extract solvent (70% acetonitrile and 0.1% formic acid in Milli-Q water) were added into 50 μL of the standards and the PK plasma samples. After extraction, the samples were centrifuged at 4500*g* for 20 min in a refrigerated centrifuge (Eppendorf 5415R) at 4 °C. 70 μL of the supernatants were transferred to a fresh 96 well-plate. Samples were analyzed using the UHPLC-1290 unit (Agilent Technologies, Singapore) coupled with a triple stage quadrupole MS unit (ABI5500Qtrap, AB Sciex, Singapore). The samples were resolved on a Kinetex C18 column (50 mm × 2.1 mm internal diameter; Phenomenex, USA) maintained at 25 °C. The mobile phase A consisted of 0.1% formic acid in deionized water, and the mobile phase B consisted of acetonitrile. The gradient program was 5% B to 95% B from 0.01 to 1.0 min, maintaining 95% B from 1.0 to 1.6 min, then switched back to 5% B from 1.65 to 2.5 min, with a constant flow rate of 0.4 mL/min. The injection volume was 2 μL. The total eluent from the liquid chromatography was injected directly into the ABI5500Qtrap mass spectrometer for analysis. MS/MS detection was operated in electrospray ionization positive ion mode. The ion spray voltage was 5.5 kV, and the vaporization temperature was set to 550 °C. The curtain gas was set at 30 (arbitrary units). The flow rates of ion source gases 1 and 2 were set at 50 (arbitrary units/min). Quantitation was carried out using the multiple reaction monitoring (MRM) of the transitions. The MS parameters for **48**-MRM were $m/z$ 490.04 → $m/z$ 295.2; collision energy, 61 V; declustering potential, 120 V; and collision cell exit, 20 V. The MS parameters for carbamazepine−MRM were $m/z$ 237.1 → $m/z$ 194.1; collision energy, 27 V; DP, 100 V; and CXP, 26 V.

*Maximum Tolerated Dose (MTD) Determination.* Female NOD-SCID mice (7−9 weeks old) were randomly in groups of three mice. They received either vehicle or a single dose of 10, 50, 100, and 200 mg/kg of **48** via oral gavage daily for 7 consecutive days. The volume of used for oral administration was 10 mL/kg. After a treatment that lasted 7 days, mice were observed for delayed clinical abnormality for another 7 days. Mice were sacrificed using $CO_2$ gas at the end of 14-day MTD study.

**Efficacy Experiments: Combination of 48 and Dasatinib.** *In Vivo Antitumor Efficacy Studies.* Dasatinib and **48** were weighed and dissolved in 0.5% MC/0.1% TW80 solution. The mixtures were vortexed and sonicated in the ultrasonic bath for 30 min. The final concentration of **48** dosing solution was 2.5, 5, and 10 mg/mL for oral dosing levels at 25, 50, and 100 mg/kg, respectively. The final concentration of dasatinib was 0.25 mg/mL for an oral dosing level at 2.5 mg/kg.

The chronic myeloid leukemic K562-eIF4E cells were obtained from Dr. Ong Sin Tiong, DUKE-NUS. They were generated by retroviral batch transfection of K562 cells (CCL-243 from the American Tissue Type Collection) with the MSCV-IRES-GFP vector_ENREF_76[75] encoding full-length murine eIF4E. The K562 transfected cells were FACS sorted for cells expressing high levels of eIF4E, which were used for xenograft studies. The K562-eIF4E cells were free of mycoplasma contamination. They were cultured in the RPMI medium supplemented with 10% fetal bovine serum (Life Technologies, Singapore) and antibiotic solution (100 units/mL penicillin and 100 μg/mL streptomycin) at 37 °C under 5% $CO_2$.

The K562-eIF4E cells ($10^7$ cells/mouse) were subcutaneously implanted into the right flank of female SCID mice. The volume of injection was 100 μL/mouse. After implantation, the tumor was monitored twice a week using a digital caliper. The K562-eIF4E tumor volume was estimated according to the following formula: Tumor volume ($mm^3$) = $(w^2 \times l)/2$, where $w$ = width and $l$ = length in mm.

When the tumors attained a volume between 75 to 196 $mm^3$, mice were randomly distributed into different groups of 8 mice per group. After randomization, mice bearing K562-eIF4E tumors received vehicle (0.5% MC/0.1% TW80) or **48** once daily for 14 days (qd × 14); or dasatinib for two cycles of 5 days on and 2 days off schedule (5d On_2d Off × 2) via oral gavage. For combination drugs treatment group, mice received dasatinib followed by **48** at 1 h post dasatinib dose. The schedule used for combination drug treatment was the same as dasatinib monotherapy (5d On_2d Off × 2) and **48** monotherapy (qd × 14). The volume of oral administration was 10 mL/kg. The dosing levels for **48** were 25, 50, and 100 mg/kg. The dosing level of dasatinib was 2.5 mg/kg. The dosing levels for dasatinib and **48** combination therapy were 2.5 mg/kg and 25, 50, or 100 mg/kg.

The end point used to measure the response of the K562-eIF4E tumors after compound treatment was tumor growth inhibition at day 14 and was expressed as %TGI and $T/C$ ratio. The percentage of tumor growth inhibition (%TGI) was calculated as follows: %TGI = $(C_{\text{day a}} - T_{\text{day a}})/(C_{\text{day a}} - C_{\text{day 1}}) \times 100$, where $C_{\text{day a}}$ = mean tumor volume of the vehicle control group at the indicated day a; $T_{\text{day a}}$ = mean tumor volume of the group treated with the test compound at the indicated day a; and $C_{\text{day 1}}$ = mean tumor volume of the vehicle control group at Day 1. The $T/C$ ratio was calculated as follows: $T/C$ ratio = $T_{\text{day a}}/C_{\text{day a}}$.

One-way ANOVA followed by Bonferroni Multiple Comparison Test was used to determine statistically significant differences between:

- the tumor volumes of the vehicle control group, and the tumor volumes of the dasatinib monotherapy group, the **48** monotherapy group, or the dasatinib and **48** combination therapy group;
- the tumor volumes of the dasatinib monotherapy group, and the tumor volumes of the dasatinib and **48** combination therapy group;
- the tumor volumes of the **48** monotherapy group, and the tumor volumes of the dasatinib and **48** combination therapy group.

GraphPad Prism version 5.1 was used for all statistical analyses.

*Western Blot.* K562-eIF4E tumor mouse model was established with CB17 SCID mice. Single dose of 100 mg/kg of **48** and 2.5 mg/kg of dasatinib was orally administered. The mice were sacrificed at the stated time point (predose, 1 h, 4 h, and 8 h after compound was administered), and the tumor was excised and flash frozen in liquid nitrogen. The tumor was homogenized three times at 3000 rpm for 5 min in RipaBuffer containing SDS, a cocktail of protease and phosphatase inhibitor (Santa Cruz Biotechnology, Inc.), and stainless steel beads with a TOMY MS-100 homogenizer. The lysate was clarified via 2 rounds of centrifugation at 13 200 rpm for 15 min at a temperature of 4 °C. The lysates were quantitated with Quick Start Bradford Protein Assay (Bio-Rad) and denatured by boiling with 2× Laemmli sample buffer supplemented with β-mercaptoethanol (Bio-Rad) for 10 min. Equal amounts of protein were loaded and separated using the NuPAGE Novex 4−12% gradient. Bis-Tris Protein Gel (Life Technologies) and subsequently transferred to a nitrocellulose membrane. Membrane was blocked for 1 h at room temperature in 5% w/v BSA in PBST. Incubation with primary antibody (anti-eIF4E abcam#130210, anti-eIF4E phospho-S209 abcam#4774, anti-pCRKL cell signaling#3181, anti-CRKL cell signaling#3182, anti-GAPDH AM#4300) were performed overnight at 4 °C followed by secondary antibody (ECL anti-mouse IgG-HRP, GE Healthcare #NA9310 or ECL-anti-rabbit IgG-HRP, GE Healthcare #NA9340) incubation for 1 h at room temperature. ECL-Plus (Amersham #RPN2235) was used for Western blot detection using the FluorChem R Imaging system (ProteinSimple) Chemiluminescent channel.

## ■ ASSOCIATED CONTENT

### Supporting Information

The Supporting Information is available free of charge on the ACS Publications Web site at DOI: The Supporting Information is available free of charge on the ACS Publications website at DOI: 10.1021/acs.jmedchem.7b01714.



DOI: 10.1021/acs.jmedchem.7b01714
J. Med. Chem. 2018, 61, 4348−4369

Analysis of molecular dynamics of MNK2 with compound **4** (PDF)
Analysis of molecular dynamics of MNK2 with compound **27** (PDF)
Analysis of molecular dynamics of MNK2 with compound **45** (PDF)
SMILES strings (CSV)
Table S1, compounds with substitution at the 2 and 8 positions; Table S2, inactive C-3 heterocycles; Table S3, tetrazole replacement; Table S4, mouse pharmacokinetics data after p.o. administration for compounds **27**, **33**, and **37**; Table S5, selectivity screen of CGP-57380 and cercosporamide and **27** tested against a panel of 104 kinases; Table S6, other bicyclic cores; Table S7, CellTiter-Glo viability assay screen against 25 cell lines; Table S8, single agents and combination studies using **48** (ETC-206) and/or dasatinib on K562 mouse xenograft model; Figure S1, *in vivo* biomarker analysis of compound **48** and dasatinib combination on eIF4E and CRKL; microsomal stability determination; Cyp inhibition ($IC_{50}$) determination; LogD determination; mouse and human PPB determination; and Caco-2 permeability (PDF)

## AUTHOR INFORMATION


### Corresponding Author

*Tel: +65 6407 0343. Fax: +65 6478 8768. E-mail: knacro@etc.a-star.edu.sg.

### ORCID

Srinivasaraghavan Kannan: 0000-0002-9539-5249
Chandra S. Verma: 0000-0003-0733-9798
Anders Poulsen: 0000-0002-2790-9340
Kassoum Nacro: 0000-0002-3291-0215


### Author Contributions

The manuscript was written through contributions of all authors. All authors have given approval to the final version of the manuscript.

### Notes

The authors declare the following competing financial interest(s): All authors (except Chandra Verma) are current or former employees of the Experimental Therapeutics Centre or Duke-NUS Graduate Medical School Singapore. Both institutes have a commercial interest in the development of MNK1/2 inhibitors.

## ACKNOWLEDGMENTS

We are thankful to Dr. Thomas Keller for helpful discussions in preparation of this manuscript. This work was financially supported by Biomedical Sciences Institutes (BMSI) and Joint Council Office (JCO Project 11 03 FG 07 05), Agency for Science, Technology and Research (A*STAR), Singapore, which is gratefully acknowledged. We thank Dr. Subir Sadhukhan and his team at AMRI Hyderabad, and Dr. Joseph Shambabu Maddirala and Dr. Sreenivasa Reddy Anugu and his team at GVK Biosciences, for the synthesis of compounds. We also thank Sudhir Tiwari and Dr. Pratima Srivastava at GVK Biosciences for compounds ADME and physiochemical properties determination.

## ABBREVIATIONS USED

BC, blast crisis; CP, chronic phase; LSC, leukemic stem cell; CML, chronic myeloid leukemia; MNK, mitogen-activated protein kinase interacting kinase; eIF4E, eukaryotic translation initiation factor 4E; CYP, cytochrome P450; LSCs, leukemic stem cells

## REFERENCES


(1) Joshi, S.; Platanias, L. C. Mnk kinase pathway: Cellular functions and biological outcomes. *World J. Biol. Chem.* **2014**, *5* (3), 321−333.
(2) Ueda, T.; Watanabe-Fukunaga, R.; Fukuyama, H.; Nagata, S.; Fukunaga, R. Mnk2 and Mnk1 are essential for constitutive and inducible phosphorylation of eukaryotic initiation factor 4E but not for cell growth or development. *Mol. Cell. Biol.* **2004**, *24* (15), 6539−6549.
(3) Rowlett, R. M.; Chrestensen, C. A.; Nyce, M.; Harp, M. G.; Pelo, J. W.; Cominelli, F.; Ernst, P. B.; Pizarro, T. T.; Sturgill, T. W.; Worthington, M. T. MNK kinases regulate multiple TLR pathways and innate proinflammatory cytokines in macrophages. *Am. J. Physiol. Gastrointest. Liver Physiol.* **2008**, *294* (2), G452−459.
(4) Andersson, K.; Sundler, R. Posttranscriptional regulation of TNFalpha expression via eukaryotic initiation factor 4E (eIF4E) phosphorylation in mouse macrophages. *Cytokine+* **2006**, *33* (1), 52−57.
(5) Buxade, M.; Parra, J. L.; Rousseau, S.; Shpiro, N.; Marquez, R.; Morrice, N.; Bain, J.; Espel, E.; Proud, C. G. The Mnks are novel components in the control of TNF alpha biosynthesis and phosphorylate and regulate hnRNP A1. *Immunity* **2005**, *23* (2), 177−189.
(6) Gkogkas, C. G.; Khoutorsky, A.; Cao, R.; Jafarnejad, S. M.; Prager-Khoutorsky, M.; Giannakas, N.; Kaminari, A.; Fragkouli, A.; Nader, K.; Price, T. J.; Konicek, B. W.; Graff, J. R.; Tzinia, A. K.; Lacaille, J. C.; Sonenberg, N. Pharmacogenetic inhibition of eIF4E-dependent Mmp9 mRNA translation reverses fragile X syndrome-like phenotypes. *Cell Rep.* **2014**, *9* (5), 1742−1755.
(7) Grzmil, M.; Seebacher, J.; Hess, D.; Behe, M.; Schibli, R.; Moncayo, G.; Frank, S.; Hemmings, B. A. Inhibition of MNK pathways enhances cancer cell response to chemotherapy with Temozolomide and targeted radionuclide therapy. *Cell. Signalling* **2016**, *28* (9), 1412−1421.
(8) Grzmil, M.; Morin, P., Jr.; Lino, M. M.; Merlo, A.; Frank, S.; Wang, Y.; Moncayo, G.; Hemmings, B. A. MAP kinase-interacting kinase 1 regulates SMAD2-dependent TGF-beta signaling pathway in human glioblastoma. *Cancer Res.* **2011**, *71* (6), 2392−2402.
(9) Bell, J. B.; Eckerdt, F. D.; Alley, K.; Magnusson, L. P.; Hussain, H.; Bi, Y.; Arslan, A. D.; Clymer, J.; Alvarez, A. A.; Goldman, S.; Cheng, S. Y.; Nakano, I.; Horbinski, C.; Davuluri, R. V.; James, C. D.; Platanias, L. C. MNK inhibition disrupts mesenchymal glioma stem cells and prolongs survival in a mouse model of glioblastoma. *Mol. Cancer Res.* **2016**, *14* (10), 984−993.
(10) Chrestensen, C. A.; Shuman, J. K.; Eschenroeder, A.; Worthington, M.; Gram, H.; Sturgill, T. W. MNK1 and MNK2 regulation in HER2-overexpressing breast cancer lines. *J. Biol. Chem.* **2007**, *282* (7), 4243−4252.
(11) Wheater, M. J.; Johnson, P. W.; Blaydes, J. P. The role of MNK proteins and eIF4E phosphorylation in breast cancer cell proliferation and survival. *Cancer Biol. Ther.* **2010**, *10* (7), 728−735.
(12) Nasr, Z.; Robert, F.; Porco, J. A., Jr.; Muller, W. J.; Pelletier, J. EIF4F suppression in breast cancer affects maintenance and progression. *Oncogene* **2013**, *32* (7), 861−871.
(13) Adesso, L.; Calabretta, S.; Barbagallo, F.; Capurso, G.; Pilozzi, E.; Geremia, R.; Delle Fave, G.; Sette, C. Gemcitabine triggers a pro-survival response in pancreatic cancer cells through activation of the MNK2/eIF4E pathway. *Oncogene* **2013**, *32* (23), 2848−2857.
(14) Kumar, K.; Chow, C. R.; Ebine, K.; Arslan, A. D.; Kwok, B.; Bentrem, D. J.; Eckerdt, F. D.; Platanias, L. C.; Munshi, H. G. Differential regulation of ZEB1 and EMT by MAPK-interacting protein kinases (MNK) and eIF4E in pancreatic cancer. *Mol. Cancer Res.* **2016**, *14* (2), 216−227.



DOI: 10.1021/acs.jmedchem.7b01714
*J. Med. Chem.* 2018, 61, 4348−4369

(15) Altman, J. K.; Glaser, H.; Sassano, A.; Joshi, S.; Ueda, T.; Watanabe-Fukunaga, R.; Fukunaga, R.; Tallman, M. S.; Platanias, L. C. Negative regulatory effects of Mnk kinases in the generation of chemotherapy-induced antileukemic responses. *Mol. Pharmacol.* **2010**, *78* (4), 778−784.
(16) Jamieson, C. H.; Ailles, L. E.; Dylla, S. J.; Muijtjens, M.; Jones, C.; Zehnder, J. L.; Gotlib, J.; Li, K.; Manz, M. G.; Keating, A.; Sawyers, C. L.; Weissman, I. L. Granulocyte-macrophage progenitors as candidate leukemic stem cells in blast-crisis CML. *N. Engl. J. Med.* **2004**, *351* (7), 657−667.
(17) Ly, C.; Arechiga, A. F.; Melo, J. V.; Walsh, C. M.; Ong, S. T. Bcr-Abl kinase modulates the translation regulators ribosomal protein S6 and 4E-BP1 in chronic myelogenous leukemia cells via the mammalian target of rapamycin. *Cancer Res.* **2003**, *63* (18), 5716−5722.
(18) Prabhu, S.; Saadat, D.; Zhang, M.; Halbur, L.; Fruehauf, J. P.; Ong, S. T. A novel mechanism for Bcr-Abl action: Bcr-Abl-mediated induction of the eIF4F translation initiation complex and mRNA translation. *Oncogene* **2007**, *26* (8), 1188−1200.
(19) Landon, A. L.; Muniandy, P. A.; Shetty, A. C.; Lehrmann, E.; Volpon, L.; Houng, S.; Zhang, Y.; Dai, B.; Peroutka, R.; Mazan-Mamczarz, K.; Steinhardt, J.; Mahurkar, A.; Becker, K. G.; Borden, K. L.; Gartenhaus, R. B. MNKs act as a regulatory switch for eIF4E1 and eIF4E3 driven mRNA translation in DLBCL. *Nat. Commun.* **2014**, *5*, 5413.
(20) Pelletier, J.; Graff, J.; Ruggero, D.; Sonenberg, N. Targeting the eIF4F translation initiation complex: a critical nexus for cancer development. *Cancer Res.* **2015**, *75* (2), 250−263.
(21) Furic, L.; Rong, L.; Larsson, O.; Koumakpayi, I. H.; Yoshida, K.; Brueschke, A.; Petroulakis, E.; Robichaud, N.; Pollak, M.; Gaboury, L. A.; Pandolfi, P. P.; Saad, F.; Sonenberg, N. eIF4E phosphorylation promotes tumorigenesis and is associated with prostate cancer progression. *Proc. Natl. Acad. Sci. U. S. A.* **2010**, *107* (32), 14134−14139.
(22) Zhang, M.; Fu, W.; Prabhu, S.; Moore, J. C.; Ko, J.; Kim, J. W.; Druker, B. J.; Trapp, V.; Fruehauf, J.; Gram, H.; Fan, H. Y.; Ong, S. T. Inhibition of polysome assembly enhances imatinib activity against chronic myelogenous leukemia and overcomes imatinib resistance. *Mol. Cell. Biol.* **2008**, *28* (20), 6496−6509.
(23) American Cancer Society. Treating Chronic Myeloid Leukemia by Phase. http://www.cancer.org/cancer/leukemia-chronicmyeloidcml/detailedguide/leukemia-chronic-myeloid-myelogenous-treating-treating-by-phase (accessed Aug 5, 2015).
(24) Corbin, A. S.; Agarwal, A.; Loriaux, M.; Cortes, J.; Deininger, M. W.; Druker, B. J. Human chronic myeloid leukemia stem cells are insensitive to imatinib despite inhibition of BCR-ABL activity. *J. Clin. Invest.* **2011**, *121* (1), 396−409.
(25) Wieczorek, A.; Uharek, L. Management of Chronic Myeloid Leukemia Patients Resistant to Tyrosine Kinase Inhibitors Treatment. *Biomarker Insights* **2015**, *10* (Suppl3), 49−54.
(26) Eiring, A. M.; Khorashad, J. S.; Anderson, D. J.; Yu, F.; Redwine, H. M.; Mason, C. C.; Reynolds, K. R.; Clair, P. M.; Gantz, K. C.; Zhang, T. Y.; Pomicter, A. D.; Kraft, I. L.; Bowler, A. D.; Johnson, K.; Partlin, M. M.; O'Hare, T.; Deininger, M. W. Beta-catenin is required for intrinsic but not extrinsic BCR-ABL1 kinase-independent resistance to tyrosine kinase inhibitors in chronic myeloid leukemia. *Leukemia* **2015**, *29* (12), 2328−2337.
(27) Topisirovic, I.; Guzman, M. L.; McConnell, M. J.; Licht, J. D.; Culjkovic, B.; Neering, S. J.; Jordan, C. T.; Borden, K. L. Aberrant eukaryotic translation initiation factor 4E-dependent mRNA transport impedes hematopoietic differentiation and contributes to leukemogenesis. *Mol. Cell. Biol.* **2003**, *23* (24), 8992−9002.
(28) Lim, S.; Saw, T. Y.; Zhang, M.; Janes, M. R.; Nacro, K.; Hill, J.; Lim, A. Q.; Chang, C. T.; Fruman, D. A.; Rizzieri, D. A.; Tan, S. Y.; Fan, H.; Chuah, C. T.; Ong, S. T. Targeting of the MNK-eIF4E axis in blast crisis chronic myeloid leukemia inhibits leukemia stem cell function. *Proc. Natl. Acad. Sci. U. S. A.* **2013**, *110* (25), E2298−2307.
(29) Perl, A.; Carroll, M. BCR-ABL kinase is dead; long live the CML stem cell. *J. Clin. Invest.* **2011**, *121* (1), 22−25.
(30) Sands, W. A.; Copland, M.; Wheadon, H. Targeting self-renewal pathways in myeloid malignancies. *Cell Commun. Signaling* **2013**, *11* (1), 33.
(31) Li, Z.; Sun, Y.; Qu, M.; Wan, H.; Cai, F.; Zhang, P. Inhibiting the MNK-eIF4E-beta-catenin axis increases the responsiveness of aggressive breast cancer cells to chemotherapy. *Oncotarget* **2017**, *8* (2), 2906−2915.
(32) Xu, H.; Wang, Z.; Xu, L.; Mo, G.; Duan, G.; Wang, Y.; Sun, Z.; Chen, H. Targeting the eIF4E/beta-catenin axis sensitizes cervical carcinoma squamous cells to chemotherapy. *Am. J. Transl. Res.* **2017**, *9* (3), 1203−1212.
(33) Hehlmann, R. How I treat CML blast crisis. *Blood* **2012**, *120* (4), 737−747.
(34) Dreas, A.; Mikulski, M.; Milik, M.; Fabritius, C. H.; Brzozka, K.; Rzymski, T. Mitogen-activated protein kinase (MAPK) interacting kinases 1 and 2 (MNK1 and MNK2) as targets for cancer therapy: recent progress in the development of MNK inhibitors. *Curr. Med. Chem.* **2017**, *24* (28), 3025−3053.
(35) Hou, J.; Lam, F.; Proud, C.; Wang, S. Targeting Mnks for cancer therapy. *Oncotarget* **2012**, *3* (2), 118−131.
(36) Tschopp, C.; Knauf, U.; Brauchle, M.; Zurini, M.; Ramage, P.; Glueck, D.; New, L.; Han, J.; Gram, H. Phosphorylation of eIF-4E on Ser 209 in response to mitogenic and inflammatory stimuli is faithfully detected by specific antibodies. *Mol. Cell Biol. Res. Commun.* **2000**, *3* (4), 205−211.
(37) Knauf, U.; Tschopp, C.; Gram, H. Negative regulation of protein translation by mitogen-activated protein kinase-interacting kinases 1 and 2. *Mol. Cell. Biol.* **2001**, *21* (16), 5500−5511.
(38) Ishida, M.; Ishida, T.; Nakashima, H.; Miho, N.; Miyagawa, K.; Chayama, K.; Oshima, T.; Kambe, M.; Yoshizumi, M. Mnk1 is required for angiotensin II-induced protein synthesis in vascular smooth muscle cells. *Circ. Res.* **2003**, *93* (12), 1218−1224.
(39) Konicek, B. W.; Stephens, J. R.; McNulty, A. M.; Robichaud, N.; Peery, R. B.; Dumstorf, C. A.; Dowless, M. S.; Iversen, P. W.; Parsons, S.; Ellis, K. E.; McCann, D. J.; Pelletier, J.; Furic, L.; Yingling, J. M.; Stancato, L. F.; Sonenberg, N.; Graff, J. R. Therapeutic inhibition of MAP kinase interacting kinase blocks eukaryotic initiation factor 4E phosphorylation and suppresses outgrowth of experimental lung metastases. *Cancer Res.* **2011**, *71* (5), 1849−1857.
(40) Teo, T.; Yang, Y.; Yu, M.; Basnet, S. K.; Gillam, T.; Hou, J.; Schmid, R. M.; Kumarasiri, M.; Diab, S.; Albrecht, H.; Sykes, M. J.; Wang, S. An integrated approach for discovery of highly potent and selective Mnk inhibitors: Screening, synthesis and SAR analysis. *Eur. J. Med. Chem.* **2015**, *103*, 539−550.
(41) Diab, S.; Teo, T.; Kumarasiri, M.; Li, P.; Yu, M.; Lam, F.; Basnet, S. K.; Sykes, M. J.; Albrecht, H.; Milne, R.; Wang, S. Discovery of 5-(2-(phenylamino)pyrimidin-4-yl)thiazol-2(3H)-one derivatives as potent Mnk2 inhibitors: synthesis, SAR analysis and biological evaluation. *ChemMedChem* **2014**, *9* (5), 962−972.
(42) Kosciuczuk, E. M.; Saleiro, D.; Kroczynska, B.; Beauchamp, E. M.; Eckerdt, F.; Blyth, G. T.; Abedin, S. M.; Giles, F. J.; Altman, J. K.; Platanias, L. C. Merestinib blocks Mnk kinase activity in acute myeloid leukemia progenitors and exhibits antileukemic effects in vitro and in vivo. *Blood* **2016**, *128* (3), 410−414.
(43) Teo, T.; Yu, M.; Yang, Y.; Gillam, T.; Lam, F.; Sykes, M. J.; Wang, S. Pharmacologic co-inhibition of Mnks and mTORC1 synergistically suppresses proliferation and perturbs cell cycle progression in blast crisis-chronic myeloid leukemia cells. *Cancer Lett.* **2015**, *357* (2), 612−623.
(44) Teo, T.; Lam, F.; Yu, M.; Yang, Y.; Basnet, S. K.; Albrecht, H.; Sykes, M. J.; Wang, S. Pharmacologic inhibition of MNKs in acute myeloid leukemia. *Mol. Pharmacol.* **2015**, *88* (2), 380−389.
(45) Han, W.; Ding, Y.; Xu, Y.; Pfister, K.; Zhu, S.; Warne, B.; Doyle, M.; Aikawa, M.; Amiri, P.; Appleton, B.; Stuart, D. D.; Fanidi, A.; Shafer, C. M. Discovery of a selective and potent inhibitor of mitogen-activated protein kinase-interacting kinases 1 and 2 (MNK1/2) utilizing structure-based drug design. *J. Med. Chem.* **2016**, *59* (7), 3034−3045.


DOI: 10.1021/acs.jmedchem.7b01714
*J. Med. Chem.* 2018, 61, 4348−4369

(46) Eis, K. Amino-Substituted Imidazopyridazines. WO/2013/034570, March 14, 2013.
(47) Eis, K. P. F.; Zorn, L.; Scholz, A.; Lienau, P.; Gnoth, M. J.; Bömer, U.; Günther, J.; Hitchcock, M. Amino-Substituted Imidazopyridazines. WO/2013/087581, June 20, 2013.
(48) National Institutes of Health, U.S. National Library of Medicine. Phase I Dose Escalation and Expansion of Oral BAY 1143269 in Combination With Intravenous Docetaxel. https://clinicaltrials.gov/ct2/show/NCT02439346 (accessed February 2, 2018).
(49) Webster, K. R.; Goel, V. K.; Hung, I. N.; Parker, G. S.; Staunton, J.; Neal, M.; Molter, J.; Chiang, G. G.; Jessen, K. A.; Wegerski, C. J.; Sperry, S.; Huang, V.; Chen, J.; Thompson, P. A.; Appleman, J. R.; Webber, S. E.; Sprengeler, P. A.; Reich, S. H. eFT508, a potent and selective mitogen-activated protein kinase interacting kinase (MNK) 1 and 2 inhibitor, is efficacious in preclinical models of diffuse large b-cell lymphoma (DLBCL). *Blood* **2015**, *126* (23), 1554−1554.
(50) Webster, K. R. eFT508: An oral, potent and highly selective inhibitor of mitogen-activated protein kinase interacting kinase (MNK) 1 and 2, a novel approach for the treatment of cancer. Presented at the Annual Meeting of the American Association for Cancer Research, New Orleans, 2016.
(51) Reich, S. H.; Sprengeler, P. A.; Chiang, G. G.; Appleman, J. R.; Chen, J.; Clarine, J.; Eam, B.; Ernst, J. T.; Han, Q.; Goel, V. K.; Han, E. Z.; Huang, V.; Hung, I. N.; Jemison, A.; Jessen, K. A.; Molter, J.; Murphy, D.; Neal, M.; Parker, G. S.; Shaghafi, M.; Sperry, S.; Staunton, J.; Stumpf, C. R.; Thompson, P. A.; Tran, C.; Webber, S. E.; Wegerski, C. J.; Zheng, H.; Webster, K. R. Structure-based design of pyridone-aminal eFT508 targeting dysregulated translation by selective mitogen-activated protein kinase interacting kinases 1 and 2 (MNK1/2) inhibition. *J. Med. Chem.* **2018**, *61*, 3516−3540.
(52) Cherian, J.; Nacro, K.; Poh, Z. Y.; Guo, S.; Jeyaraj, D. A.; Wong, Y. X.; Ho, M.; Yang, H. Y.; Joy, J. K.; Kwek, Z. P.; Liu, B.; Wee, J. L.; Ong, E. H.; Choong, M. L.; Poulsen, A.; Lee, M. A.; Pendharkar, V.; Ding, L. J.; Manoharan, V.; Chew, Y. S.; Sangthongpitag, K.; Lim, S.; Ong, S. T.; Hill, J.; Keller, T. H. Structure-activity relationship studies of mitogen activated protein kinase interacting kinase (MNK) 1 and 2 and BCR-ABL1 inhibitors targeting chronic myeloid leukemic cells. *J. Med. Chem.* **2016**, *59* (7), 3063−3078.
(53) Oyarzabal, J.; Zarich, N.; Albarran, M. I.; Palacios, I.; Urbano-Cuadrado, M.; Mateos, G.; Reymundo, I.; Rabal, O.; Salgado, A.; Corrionero, A.; Fominaya, J.; Pastor, J.; Bischoff, J. R. Discovery of mitogen-activated protein kinase-interacting kinase 1 inhibitors by a comprehensive fragment-oriented virtual screening approach. *J. Med. Chem.* **2010**, *53* (18), 6618−6628.
(54) Jauch, R.; Jakel, S.; Netter, C.; Schreiter, K.; Aicher, B.; Jackle, H.; Wahl, M. C. Crystal structures of the Mnk2 kinase domain reveal an inhibitory conformation and a zinc binding site. *Structure* **2005**, *13* (10), 1559−1568.
(55) Jauch, R.; Cho, M. K.; Jakel, S.; Netter, C.; Schreiter, K.; Aicher, B.; Zweckstetter, M.; Jackle, H.; Wahl, M. C. Mitogen-activated protein kinases interacting kinases are autoinhibited by a reprogrammed activation segment. *EMBO J.* **2006**, *25* (17), 4020−4032.
(56) Choi, H. S.; Rucker, P. V.; Wang, Z.; Fan, Y.; Albaugh, P.; Chopiuk, G.; Gessier, F.; Sun, F.; Adrian, F.; Liu, G.; Hood, T.; Li, N.; Jia, Y.; Che, J.; McCormack, S.; Li, A.; Li, J.; Steffy, A.; Culazzo, A.; Tompkins, C.; Phung, V.; Kreusch, A.; Lu, M.; Hu, B.; Chaudhary, A.; Prashad, M.; Tuntland, T.; Liu, B.; Harris, J.; Seidel, H. M.; Loren, J.; Molteni, V. (R)-2-Phenylpyrrolidine substituted imidazopyridazines: a new class of potent and selective pan-TRK inhibitors. *ACS Med. Chem. Lett.* **2015**, *6* (5), 562−567.
(57) Roux, P. P.; Blenis, J. ERK and p38 MAPK-activated protein kinases: a family of protein kinases with diverse biological functions. *Microbiol. Mol. Biol. Rev.* **2004**, *68* (2), 320−344.
(58) www.schrodinger.com (accessed July 8, 2012).
(59) Desiraju, G. R.; Steiner, T. *The Weak Hydrogen Bond: In Structural Chemistry and Biology*; Oxford Scholarship Online; Oxford University Press, 2001; p 507.
(60) Zou, B.; Nagle, A.; Chatterjee, A. K.; Leong, S. Y.; Tan, L. J.; Sim, W. L.; Mishra, P.; Guntapalli, P.; Tully, D. C.; Lakshminarayana, S. B.; Lim, C. S.; Tan, Y. C.; Abas, S. N.; Bodenreider, C.; Kuhen, K. L.; Gagaring, K.; Borboa, R.; Chang, J.; Li, C.; Hollenbeck, T.; Tuntland, T.; Zeeman, A. M.; Kocken, C. H.; McNamara, C.; Kato, N.; Winzeler, E. A.; Yeung, B. K.; Diagana, T. T.; Smith, P. W.; Roland, J. Lead optimization of imidazopyrazines: a new class of antimalarial with activity on plasmodium liver stages. *ACS Med. Chem. Lett.* **2014**, *5* (8), 947−950.
(61) Matsumoto, S.; Miyamoto, N.; Hirayama, T.; Oki, H.; Okada, K.; Tawada, M.; Iwata, H.; Nakamura, K.; Yamasaki, S.; Miki, H.; Hori, A.; Imamura, S. Structure-based design, synthesis, and evaluation of imidazo[1,2-b]pyridazine and imidazo[1,2-a]pyridine derivatives as novel dual c-Met and VEGFR2 kinase inhibitors. *Bioorg. Med. Chem.* **2013**, *21* (24), 7686−7698.
(62) Oguro, Y.; Cary, D. R.; Miyamoto, N.; Tawada, M.; Iwata, H.; Miki, H.; Hori, A.; Imamura, S. Design, synthesis, and evaluation of novel VEGFR2 kinase inhibitors: discovery of [1,2,4]triazolo[1,5-a]pyridine derivatives with slow dissociation kinetics. *Bioorg. Med. Chem.* **2013**, *21* (15), 4714−4729.
(63) Kannan, S.; Poulsen, A.; Yang, H. Y.; Ho, M.; Ang, S. H.; Eldwin, T. S.; Jeyaraj, D. A.; Chennamaneni, L. R.; Liu, B.; Hill, J.; Verma, C. S.; Nacro, K. Probing the binding mechanism of Mnk inhibitors by docking and molecular dynamics simulations. *Biochemistry* **2015**, *54* (1), 32−46.
(64) Karaman, M. W.; Herrgard, S.; Treiber, D. K.; Gallant, P.; Atteridge, C. E.; Campbell, B. T.; Chan, K. W.; Ciceri, P.; Davis, M. I.; Edeen, P. T.; Faraoni, R.; Floyd, M.; Hunt, J. P.; Lockhart, D. J.; Milanov, Z. V.; Morrison, M. J.; Pallares, G.; Patel, H. K.; Pritchard, S.; Wodicka, L. M.; Zarrinkar, P. P. A quantitative analysis of kinase inhibitor selectivity. *Nat. Biotechnol.* **2008**, *26* (1), 127−132.
(65) Bain, J.; Plater, L.; Elliott, M.; Shpiro, N.; Hastie, C. J.; McLauchlan, H.; Klevernic, I.; Arthur, J. S.; Alessi, D. R.; Cohen, P. The selectivity of protein kinase inhibitors: a further update. *Biochem. J.* **2007**, *408* (3), 297−315.
(66) Yu, M.; Li, P.; Basnet, S. K.; Kumarasiri, M.; Diab, S.; Teo, T.; Albrecht, H.; Wang, S. Discovery of 4-(dihydropyridinon-3-yl)amino-5-methylthieno[2,3-d]pyrimidine derivatives as potent Mnk inhibitors: synthesis, structure-activity relationship analysis and biological evaluation. *Eur. J. Med. Chem.* **2015**, *95*, 116−126.
(67) Dabbah, M.; Attar-Schneider, O.; Zismanov, V.; Tartakover Matalon, S.; Lishner, M.; Drucker, L. Multiple myeloma cells promote migration of bone marrow mesenchymal stem cells by altering their translation initiation. *J. Leukocyte Biol.* **2016**, *100* (4), 761−770.
(68) Timpano, S.; Uniacke, J. Human cells cultured under physiological oxygen utilize two cap-binding proteins to recruit distinct mRNAs for translation. *J. Biol. Chem.* **2016**, *291* (20), 10772−10782.
(69) Marcus, H.; Attar-Schneider, O.; Dabbah, M.; Zismanov, V.; Tartakover-Matalon, S.; Lishner, M.; Drucker, L. Mesenchymal stem cells secretomes' affect multiple myeloma translation initiation. *Cell. Signalling* **2016**, *28* (6), 620−630.
(70) RCSB. Protein Data Bank, www.rcsb.org (accessed March 5, 2013).
(71) Harder, E.; Damm, W.; Maple, J.; Wu, C.; Reboul, M.; Xiang, J. Y.; Wang, L.; Lupyan, D.; Dahlgren, M. K.; Knight, J. L.; Kaus, J. W.; Cerutti, D. S.; Krilov, G.; Jorgensen, W. L.; Abel, R.; Friesner, R. A. OPLS3: a force field providing broad coverage of drug-like small molecules and proteins. *J. Chem. Theory Comput.* **2016**, *12* (1), 281−296.
(72) Polak, E.; Ribiere, G. Note sur la convergence de méthodes de directions conjuguées. *Rev. Franc. Informat. Recherche Opérationelle, Sér. Rouge* **1969**, *16*, 35−43.
(73) Duraiswamy, A. J.; Lee, M. A.; Madan, B.; Ang, S. H.; Tan, E. S. W.; Cheong, W. W. V.; Ke, Z.; Pendharkar, V.; Ding, L. J.; Chew, Y. S.; Manoharan, V.; Sangthongpitag, K.; Alam, J.; Poulsen, A.; Ho, S. Y.; Virshup, D. M.; Keller, T. H. Discovery and optimization of a porcupine inhibitor. *J. Med. Chem.* **2015**, *58* (15), 5889−5899.
(74) Ho, S. Y.; Alam, J.; Jeyaraj, D. A.; Wang, W.; Lin, G. R.; Ang, S. H.; Tan, E. S. W.; Lee, M. A.; Ke, Z.; Madan, B.; Virshup, D. M.; Ding, L. J.; Manoharan, V.; Chew, Y. S.; Low, C. B.; Pendharkar, V.;


DOI: 10.1021/acs.jmedchem.7b01714
*J. Med. Chem.* 2018, 61, 4348−4369

Sangthongpitag, K.; Hill, J.; Keller, T. H.; Poulsen, A. Scaffold hopping and optimization of maleimide based porcupine inhibitors. *J. Med. Chem.* **2017**, *60* (15), 6678−6692.
(75) Wendel, H. G.; Silva, R. L.; Malina, A.; Mills, J. R.; Zhu, H.; Ueda, T.; Watanabe-Fukunaga, R.; Fukunaga, R.; Teruya-Feldstein, J.; Pelletier, J.; Lowe, S. W. Dissecting eIF4E action in tumorigenesis. *Genes Dev.* **2007**, *21* (24), 3232−3237.



DOI: 10.1021/acs.jmedchem.7b01714
*J. Med. Chem.* 2018, 61, 4348−4369